POLITECNICO
MILANO 1863

SCUOLA DI INGEGNERIA INDUSTRIALE
E DELL'INFORMAZIONE

Chatter Indicator for Linear Time Periodic Systems

TESI DI LAUREA MAGISTRALE IN
MECHANICAL ENGINEERING-INGEGNERIA DI MECCANICA

Author: **Ozan BEKKI**

Student ID:	913096
Advisor:	Prof. Paolo Albertelli
Co-advisor:	Fabrizio Defant
Academic Year:	2021-22

Acknowledgments

First of all, I would like to thank my supervisor, Dr. Paolo Albertelli, for giving me the opportunity of being a member of a distinguished research team. I am also thankful for his advice and kind guidance. I also would like to express my gratitude to Fabrizio Defant for sharing his experimental data and for his sincere support. I also owe my gratitude to Ugo Malguzzi for his incomparable guidance, encouragement, friendly approach and constructive discussions.

I would like to thank Milan Rathod and Gabriele Masotti for their invaluable support, stimulating discussions and friendship. I also would like to express my gratitude to all my colleagues in the group for their help and friendly work environment. Especially, I owe my gratitude to Alberto Scolari and Luca Bernini.

I would like to thank my friends Ali, Övünç, and Mümin for always being there for me. Thanks very much to my lovely flatmates Hadi, Toka and Yalda and my dearest neighbors Dilşah and Batu for being my family members in Piacenza. Also, many thanks to all my friends in Piacenza and Milan for my happy memories in Italy. Moreover, I would like to acknowledge all my friends in Turkey for their lovely support despite the physical distance between us.

My heartfelt thanks go to my family for their endless support during my MSc. life. Dad, thanks very much for teaching me how to be strong. Mum, thanks so much for being such an amazing, understanding and supporting mother. Last but not least, my greatest thanks go to my lovely sister Dr. Gözde Bekki. Thank you very much for sharing your academic experiences, for motivating me every moment and for being an excellent sister who encourages me in every sense. I love you all!

Finally, I would like to thank myself for improving my persistence, overcoming every failure and disappointment in my life, and learning how to keep my motivation strong.

Politecnico di Milano Ozan Bekki

April 6, 2022

ABSTRACT

Regenerative chatter is one of the main limiting factors for efficiency and quality in milling. It is a complex phenomenon that can emerge rapidly depending on cutting parameters, dynamics of the machine, tool, and workpiece geometry. Developing strategies for predicting, detecting, avoiding, and suppressing chatter has always been important. Although real systems cannot be characterized as linear time-invariant systems, the methods for prediction of chatter were mainly based on time-invariant system assumption which simplifies the system and may result in neglecting essential features. The complexity of creating stability lobe diagrams and the need to involve the uncertainties occurring during the machining and the consequences of changing dynamics lead to the investigation of reliable real-time chatter detection algorithms. Since this work is based on a technique that aims to suppress the chatter by varying the machine stiffness periodically, a real-time chatter indicator that can separate the chatter frequency and the sidebands near tooth-passing frequency created due to the changing dynamics was the main focus. Therefore, another algorithm was developed for deciding the spindle speed and modulation status to specific tooth passing frequencies and possible sideband formation.

SOMMARIO

Il chatter rigenerativo è uno dei principali fattori limitanti per efficienza e qualità nella fresatura. Si tratta di un fenomeno complesso che può emergere rapidamente a seconda dei parametri di taglio, della dinamica della macchina, dell'utensile e della geometria del pezzo. Lo sviluppo di strategie per prevedere, rilevare, evitare e sopprimere il chatter è sempre stato importante. Sebbene i sistemi reali non potessero essere modellati come sistemi lineari tempo invarianti, i metodi per la previsione del chatter erano principalmente basati sull'assunzione che il sistema fosse invariante nel tempo. Questa assunzione semplificativa può portare a trascurare caratteristiche essenziali. La complessità della creazione di diagrammi di stabilità e la necessità di coinvolgere le incertezze che si verificano durante la lavorazione e le conseguenze del cambiamento delle dinamiche portano allo studio di algoritmi affidabili di rilevamento delle vibrazioni in tempo reale. Poiché questo lavoro si basa su una tecnica che mira a sopprimere le vibrazioni variando periodicamente la rigidità della macchina, il principale focus del progetto è stato lo sviluppo di un indicatore dalle vibrazioni in tempo reale in grado di separare la frequenza vibratoria di chatter dalle bande laterali vicino alla frequenza di passaggio dei denti generata a causa del cambiamento della dinamica. Pertanto, E' stato inoltre sviluppato un altro algoritmo per monitorare la velocità del mandrino e lo stato di modulazione in base alle specifiche frequenze di passaggio dei denti e alla possibile formazione di bande laterali.

Table of Contents

Tables

Figures

1 INTRODUCTION

1.1 Machine Tool Sector Overview

A "machine tool", according to the International Organization for Standardization (ISO), is a mechanical utensil that is set up and driven to shape workpieces by removing or adding material or mechanically deforming in a chosen manner. Metalworking machine tools, such as lathes, sheet metal forming machines, milling machines, grinding machines, electrical discharge machining (EDM) machines, laser cutting and additive manufacturing machines come in a wide range of technologies[1]. Accordingly, machine tools are a highly heterogeneous group of products due to the high level of customization in terms of the size and material being machined, the level of automation, speed, or performance [2]. Also, these machine tools supply products to key industries such as automotive, aerospace, energy, and medical technology.

In the last decade, the machine tool sector has seen substantial and continual changes due to the industrial revolution, Industry 4.0, or the digitalization of industry. The advancements in intelligent technologies such as new-generation sensors, advanced robotics, and artificial intelligence have changed the progress of the machine tool sector. The growing demand pushed machine tool manufacturers to produce higher quality products with extended life with the enhancement of performance optimization using the beforementioned technologies. Machine tools builders focus on producing customized, multitasking, efficient and reliable machines. They are projected on the idea of providing technical support to the customer, satisfying the principles of preventive and predictive maintenance. Another important aspect is the reduction of energy consumption and sustainability improvement; indeed, the industrial sector uses more energy than any other end-user sector, currently consuming about one-half of the total energy supplied to the world [3]. The goal in this direction is to produce environmentally friendly machines, according to the binding obligations on industrialized countries to reduce emissions of greenhouse gases as stated by the Kyoto Protocol to the United Nations Framework Convention on Climate Change.The Italian contribution in the machine tools sector is one of the most

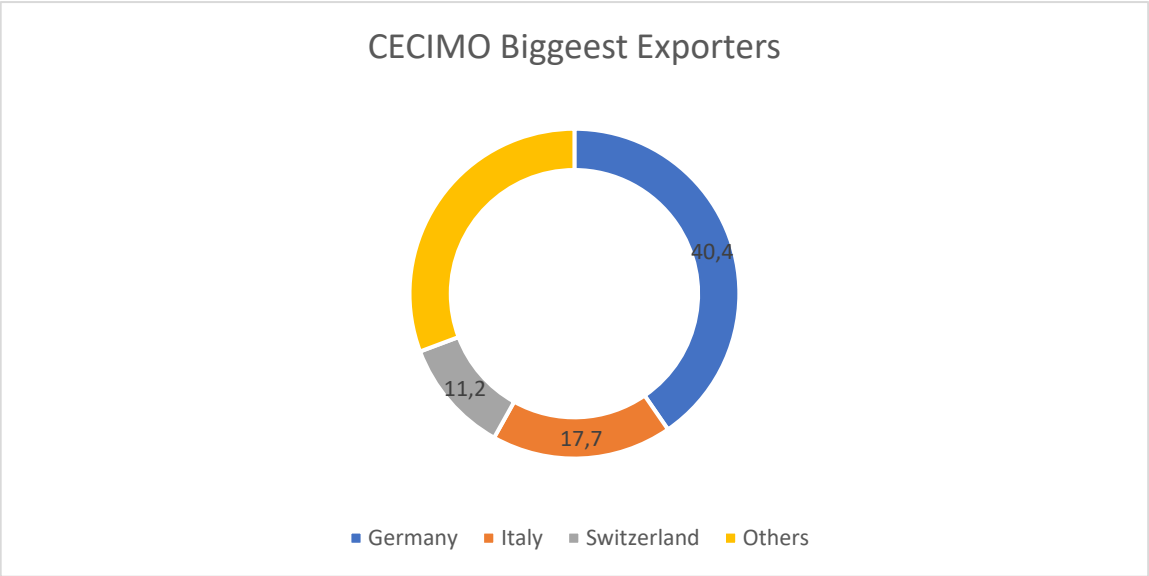

Figure 1. Role of Italy in machine tools EUROPE (CECIMO 2021)

important in Europe and in the world. As highlighted in [4], 2021 was extremely positive for the Italian industry of machine tools, robotics and automation, which reported double-digit increases for all key economic indicators. The outcome was due to the excellent trend of Italian manufacturers' deliveries in the domestic market, which increased by 27.8% to 2,965 million euro, as well as to the positive performance of exports, achieving 3,360 million euro, i.e. 17.4% more than in the previous year.

Figure 1 shows the importance of Italy in the Europe Market. The biggest exporter is Germany, followed by Italy and Switzerland along with the CECIMO members. The three countries represent two thirds of the total CECIMO output.

Based on the ISTAT data processing by UCIMU, in the period January-September 2021 (latest available data), Italian exports of machine tools only started to grow again in almost all countries of destination. Sales to Germany, which turned out to be the first country for the "Made in Italy" exports of the sector, went up to 256 million euro (+38.4%). The other major destination countries were the United States, 251 million euro (+9.7%), China, 154 million euro (- 5.3%), Poland, 118 million euro (+29%) and France, 117 million euro (+1.2%). The domestic market was extremely lively, as shown by the data of consumption, which increased by

30.4% in 2021 compared with the previous year, attaining a value of 4,645 million Euros [4].

To maintain the positive trends, the machines are becoming smarter, sensors are now available for multiple purposes and can now be integrated into every device. This is directly linked to the improvements obtained by the industrial revolution. The real-time process monitoring with the use of sensors has found a wide area of application in the machining world. Collecting useful data and making these data meaningful have become the main goal to have an accurate, efficient and more robust process. Cutting conditions influence several process factors in machining operations, including cutting forces, vibrations, surface finish, temperature etc. With the right physical sensors, these variables can be measured. Sensors are also necessary for monitoring tasks that are typically performed by humans. Internal sensor data can be used as a predictor of cutting quality, however it can also provide information on the machine's status, which can be valuable for maintenance planning, minimizing downtime, and increasing productivity. Aside from great quality, the ability to monitor the equipment ensures consistent functioning. Communication-capable machines can compensate the errors, while the combination of communication with automation is essential for high productivity, low scrap, and excellent work-piece quality. The sensor signal is tampered with to create a link between the tool and/or process state. For the final diagnosis, the data is loaded into a cognitive decision-making assistance system. Finally, based on the assessed data, the support system can give a recommendation or act. Both the human operator and the machine tool numerical controller that performs adaptive/corrective operations can undertake this final step.

1.2 Milling

Milling is a process performed with a machine in which the cutters rotate to remove the material from the work piece as in Figure 2. Milling is one of the most important and widespread machining operations, since it can guarantee high material removal rate, high complexity and precision. To achieve better accuracy and repeatability for the complex parts, CNC (Computer Numerical Control) machining was developed. This was a major step for its time, but there have been few

improvements over the years to make the system smarter. There is a need for automated process monitoring and process improvement to make CNC machining both safe and efficient. These improvements make machining process more reliable for various fields, for example automotive, aerospace, precision technology etc. where complex cuts are regularly present and, in order to obtain high productivity and quality, maximizing both material removal rate and cutting quality is extremely important. The cutting quality is related to tool dynamics. Most important variables that affects the part quality are

- Tool tip displacement
- Tool tip vibration
- Tool deflection
- Cutting forces

During the cut, since cutting tool is engaged in the workpiece and surrounded by the tool coolant and flow of chips, the sensor position should be decided carefully. Although, the most useful and reliable information would be taken from tool tip, it is limited to the cutting environment. This is the main reason why on-line process monitoring is a challenging task. In this work, machining vibration will be the main focus which is caused by lack of dynamic stiffness of the tool, tool holder, cutting tool-workpiece, workpiece-fixturing system [3]. These vibrations can be divided into three categories.

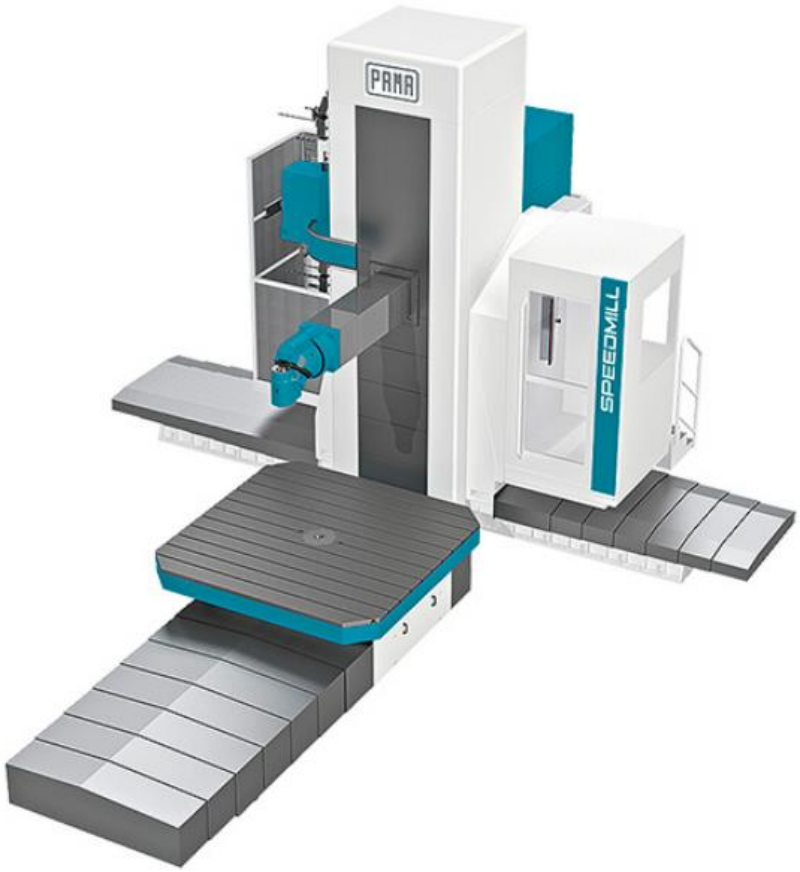

Figure 2.CNC Milling Machine-PAMA Speed Mill

- Free Vibration
- Forced vibration
- Self excited vibration

Therefore, to reduce tool damage, poor surface quality, low MRR etc., understanding the reason behind these vibrations have crucial importance to detect and suppress them.

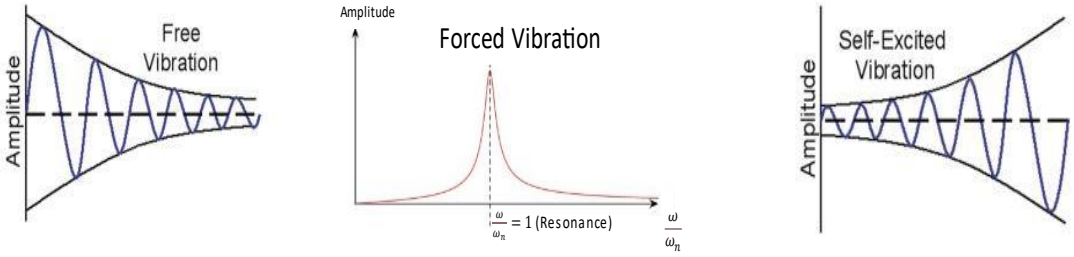

Figure 3.Vibration Classification Scheme

1.3 Vibrations during the Cutting Operations

Free vibrations result from impulses transferred to the structure through its foundation, like cutting tools' initial engagement. In other words, the primary cause of the free vibration is the sudden change of the cutting force. This vibration happens when the tool enters the workpiece, exits the workpiece, or has intermittent cutting. The deflected structure will vibrate according to its natural frequency and mode shape and die out by the damping. This nature is dependent on cutting tool geometry, workpiece geometry, and cutting conditions. For example, the helix angle of a tool can be designed to be more significant to increase the rise time of the cutting force.

Forced vibrations are produced by periodic forces acting on the system due to teeth' engagements in milling. For example, a rotating unbalanced mass or an intermittent engagement of multi-tooth cutters will excite the system with its frequency. Forced vibrations can also be caused by backlash in gear drives, inaccuracy, misalignment of machine tool parts, etc. Although the cutting forces do not generally have harmonics, assuming they are periodic, they can be decomposed as the linear combination of the Fourier series. If this frequency excitement coincides with one of the system's natural frequencies, the machine will resonate in the corresponding natural frequency. It is well known that the system response to the forced excitement is affected by the structural properties

of the dynamic system and the magnitude and frequency of the cutting force. These parameters can be changed by selecting different cutting parameters.

The last one is called self-excited vibration which is the primary problematic source of a well-known unstable cutting phenomenon called chatter. Chatter is divided into four types depending on the self-excitation mechanism. These are frictional, thermo-mechanical, mode coupling, and regenerative chatter. Frictional chatter is caused by mutual friction between the tool and the workpiece in the same direction as the cutting speed. Mode coupling chatter is caused by the coupling of two natural modes of vibration because of the slight difference between the rigidity of vibrating elements in two different directions. Thermo-mechanical chatter is due to the temperature and strain rate in the plastic deformation. Regenerative chatter is caused by differences in chip thickness resulting from the phase difference between the vibration pattern formed during a prior cutting process.[5] It grows until the tool leaves the cutting area or becomes functionless. It is a form of cutting vibration resulting from characteristics of a machining system under the ongoing aperiodic external forces. The main reason behind chatter is the regeneration of chip thickness [6]. It involves a steady energy input into the system and is caused by the interaction between the tool and the workpiece. It results in unstable cutting, poor surface finish, reduced material removal rate and damage to the machine tool. Since it brings unfavorable limiting effects to the process, problems of predicting, detecting and suppressing chatter have always taken an essential role in the machining operations [5]. Figure 4 shows the surface quality comparison between stable and unstable cut due to chatter phenomenon.

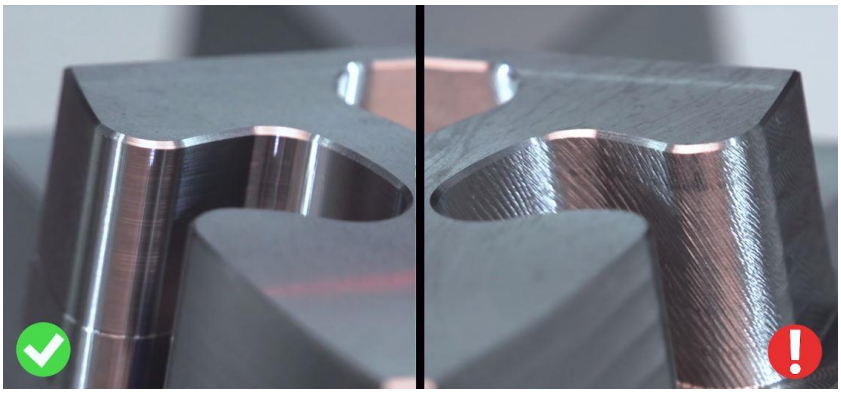

Figure 4. Chatter-free and chatter cutting surface quality comparison

The dynamic system can be shown as a block diagram in as feed-back loop block diagram as discussed in [7] and the equations will be derived in the next chapter.

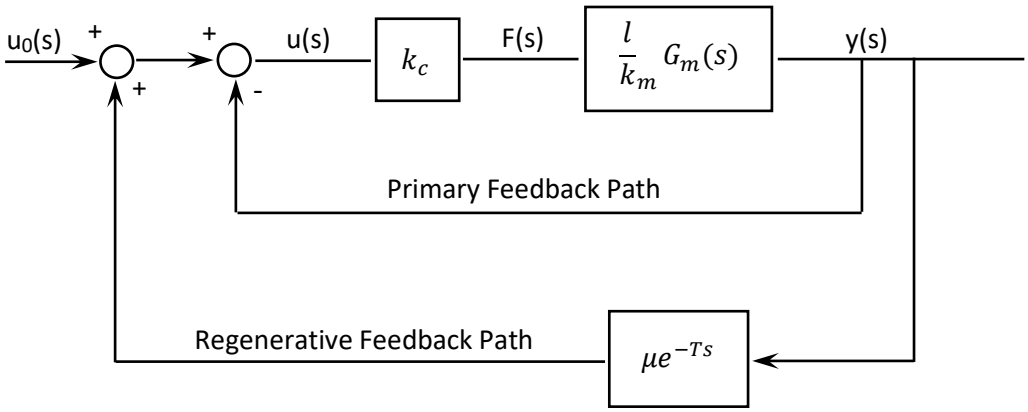

Figure 5. Block diagram of chatter

1.4 Thesis Aim and Structure

This work aims to find a real-time chatter indicator that can separate the chatter frequencies and system-related sidebands. It is crucial to understand that observing the sidebands is related to time-varying system dynamics. Therefore, system analysis, milling dynamics, and stability analysis are explained by emphasizing the LTI and LTP system differences, which is the reason behind observing the sidebands in the frequency domain and requires different solutions for stability analysis. In Chapter 3, the machining center, accelerometer, and cutting tool used during the experiments are introduced. Chapter 4 is divided into two parts. Spindle speed detection and the modulation status are specified in the pre-analysis part. Then, the methods used for developing the real-time chatter indicator are defined. The chatter indicator results obtained in parallel with the time and time-frequency analysis are shown and discussed in Chapter 5. The project's conclusion is told, and the possible improvements for the used method are explained in Chapter 6.

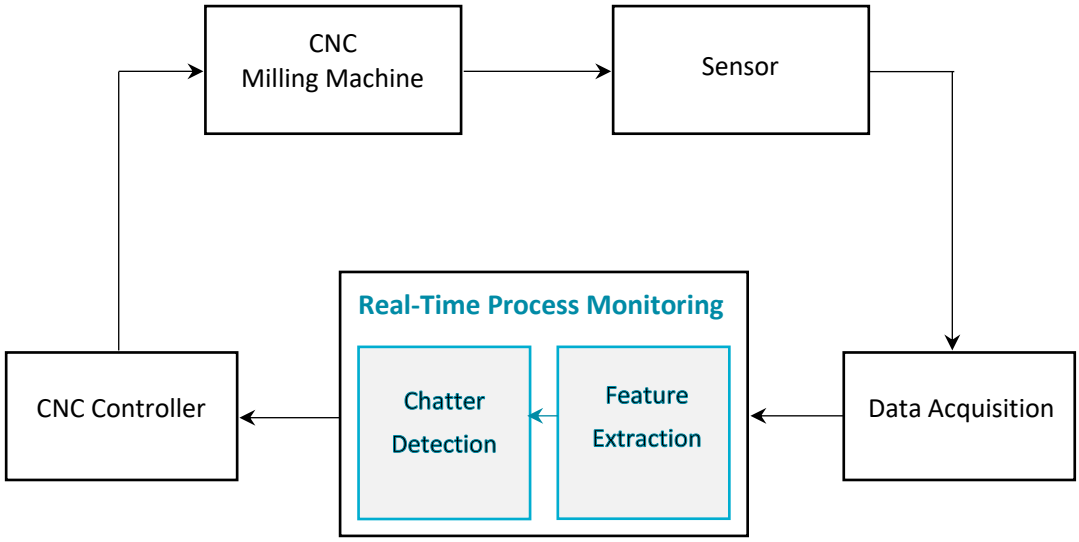

Figure 6. Structure of a machining operation

2 State of the Art

In this part, system analysis for linear time-invariant (LTI) and linear time-periodic (LTP) systems, milling parameters, milling dynamics and stability analysis for LTI and LTP systems and chatter suppression techniques will be introduced.

2.1 System Analysis

System analysis part explains the difference between the LTI and LTP systems by emphasizing the consequences of these differences such as sideband formation which is the main concern of this project.

2.1.1Linear Time-Invariant Systems

Linear time-invariant system gives response to any input excitation with the constraints of linearity and time-invariance. It is important to understand that time-invariant systems output doesn't depend on when the input was applied. This feature makes LTI system easy to represent and understand graphically. They are used to predict long term behavior of a system.

In LTI systems, if an input $u(t)$ is applied and its output $y(t)$ can be expressed as

$$y(t) = \int_{-\infty}^{\infty} g(\tau)u(t-\tau)d\tau \qquad 1$$

where $g(\tau)$ is the impulse response of the system. If exponential input $u(t) = e^{st}$ is applied, the output can be written as

$$y(t) = \int_{-\infty}^{\infty} [\![g(\tau)]\!]e^{-st}d\tau e^{st} = G(s)e^{st} \qquad 2$$

where $G(s)$ is the transfer function of linear time invariant system and $s = j\omega$. It must be recalled that if Fourier Transform is applied to the impulse response, the frequency response function (FRF) can be obtained as $G(j\omega)$. It is easy to realize

that the $G(s)\ or\ G(j\omega)$ is a linear map that shows the relation between the input and output. The state space representation is useful to represent differential equation governing dynamics of an LTI system which have constant coefficients. This is a helpful representation to show the differences between LTI and LTP systems which will be explained in next pages.

$$\dot{x}(t) = Ax(t) + Bu(t)$$

$$y(t) = Cx(t) + Du(t) \quad 3$$

In the equation above, $x(t)$ is the state vector, A is the dynamics matrix, B is the input matrix, C is the output matrix and D is the direct input matrix. According to this, the transfer function can be described as

$$G(s) = C(sI - A)^{-1}B + D \quad 4$$

2.1.2Linear Time-Periodic Systems

As said earlier, the state space representation is useful to show the differences between the LTI and LTP systems. In LTP systems, the dynamic's differential equations have time-varying and periodic coefficients.

$$\dot{x}(t) = A(t)x(t) + B(t)u(t)$$

$$y(t) = C(t)x(t) + D(t)u(t) \quad 5$$

The matrices $A(t), B(t), C(t), D(t)$ are time periodic with period T and can be shown as

$$A(t + NT) = A(t) \quad 6$$

and same for other matrices B, C and D. This difference leads to an important output change in the case of applied complex exponential or sinusoid input to an LTP system. The output will not be in the form of only input frequency ω, but a possibly infinite number of other frequencies $\omega + n\omega_p$ which ω_p is called the pumping frequency. The magnitudes and phases of each frequency have their own values [8]. In Figure 7 it can be demonstrated visually [9]. This indicates that the conventional modal identification techniques developed for LTI systems are not directly applicable to LTP systems. This drawback has led researchers to find a linear operator called harmonic transfer function that links input and output as

transfer functions of LTI systems [8]. In [10], the notion of harmonic transfer function has been discussed. It has been understood that the extension of LTI theory doesn't describe a linear operator that links complex exponential input signal to complex exponential output signal. Instead, this approach leads to a map from complex exponential signal input signals to complex exponential output signals modulated by a periodic signal. This may cause to have an infinite number of harmonics of the pumping frequency.

For all t and x(t) can be written as

$$x(t) = e^{st}\bar{x}(t) \qquad 7$$

where $s = \frac{logz}{T}$ and x(t) is periodic. The $x(t)$ is so called exponentially modulated periodic (EMP) function ad this function is the map used to describe the input-output relationship in LTP systems. The details to express exponentially modulated periodic signals can be found in [10]. EMP signals are expressed as the Fourier series of a periodic signal of ω_p to determine the transfer functions of LTP systems. With the application of Floquet theory, for all t and x(t) can be written as

$$u(t) = \sum_{-\infty}^{\infty} u_n e^{(s+in\omega_p)t} \qquad 8$$

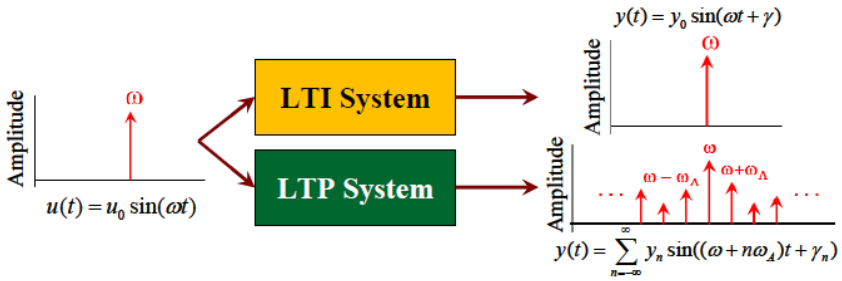

Figure 7.System response to a single frequency input

The matrices $A(t), y(t) and\, x(t)$ are substituted by EMP signals and Toeplitz transform. The Fourier coefficients of matrices $A(t)$ are organized by the expansion into a matrix with a block-Toeplitz form:

$$A_t = \begin{bmatrix} \ddots & \vdots & \vdots & \vdots & \ddots \\ \cdots & A_0 & A_{-1} & A_{-2} & \cdots \\ \cdots & A_1 & A_0 & A_{-1} & \cdots \\ \cdots & A_2 & A_1 & A_0 & \cdots \\ \ddots & \vdots & \vdots & \vdots & \ddots \end{bmatrix} \quad 9$$

where the matrix A_t is the Toeplitz transform and the procedure is same for $B(t), C(t)\ and\ D(t)$ and their transformations will be described as $B_t, C_t\ and\ D_t$. The analytical formulation of harmonic transfer function now can be defined by rearranging the terms as:

$$Y = \{C_t[sI - (A_t - N)]^{-1}B_t + D_t\}U \quad 10$$

Where N is the diagonal block matrices which include $in\omega_p I$. $Y\ and\ U$ are the Fourier coefficients of output and input respectively and can be shown as:

$$\begin{aligned} Y &= (\ldots\ Y_{-2}\ Y_{-1}\ Y_0\ Y_1\ Y_2\ \ldots)^T \\ &= \big(\ldots\ Y(\omega - 2\omega_p)\ Y(\omega - \omega_p) Y(\omega) Y(\omega + \omega_p)\ Y(\omega + 2\omega_p)\ \ldots\big)^T \end{aligned} \quad 11$$

The input-output relation is shown as above and will be used in the stability analysis of LTP systems part as a starting point.

2.2 Milling Parameters

The tool features and the cutting parameters must be defined considering milling in order to avoid terminological misunderstanding. One cutting process can be defined with the parameters cutting speed v_c, feed per tooth f_z , axial depth of cut and radial width of cut,a_p and a_e respectively.

The feed per tooth f_z is the distance covered by the tool in one rotation divided by the number of teeth. Therefore, the feed rate v_f can be formulated as

$$v_f = f_z.N.\Omega \quad 12$$

where N is the number of teeth and Ω is spindle rotational speed in RPM. The axial depth and the radial width of the cut are the engagement between the tool and workpiece as can be seen in Figure 8.

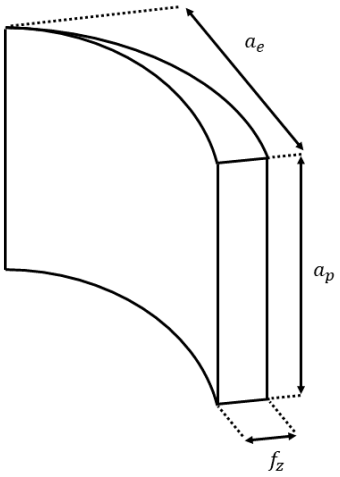

Figure 8.Sketch of a chip and parameter representation

The cutting speed v_c is defined as the tangential peripheral velocity on the cutting edges and usually defined on the maximum edge diameter as shown in Figure 9 and can be derived as in (1) where the tool diameter D is in mm. The cutting speed can be expressed as $\frac{m}{min}$.

$$v_c = \frac{\pi . \Omega . D}{1000} \qquad 13$$

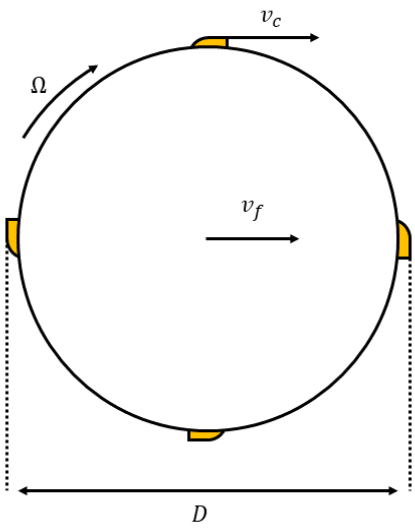

Figure 9. Cutting tool top view

All cutting operation are done with the aim of reaching required quality with the lowest cost. The cost is related to material removal rate (MRR) of the process and it is a direct indicator of efficiency of the cut. It can be defined as below

$$MRR = a_p a_e v_f \quad 14$$

2.3 Milling Dynamics

In this part, milling dynamics are explained both for LTI and LTP systems which is important to understand effects of variables on cutting force and tool displacement accordingly tool life and surface quality.

2.3.1 Linear Time-Invariant System

A milling cutter with N teeth and assumed to have zero helix angle is considered to have two orthogonal degrees of freedom in the x and y directions. The reason behind displacements in the x and y directions is the excitement due to the cutting forces. The dynamic displacements are associated with rotating tooth number (j) in the radial or chip thickness direction with the coordinate transformation of $V_j = -x\,sin\,\phi_j - y\,cos\,\phi_j$ where the ϕ_j is the instantaneous angular immersion of tooth (j) measured clockwise from Y axis [11]. This angle can be defined as $\varphi_j(t) = \left(\frac{2\pi\Omega}{60}\right) + j\frac{2\pi}{n}$ where t and Ω are time and spindle speed respectively.

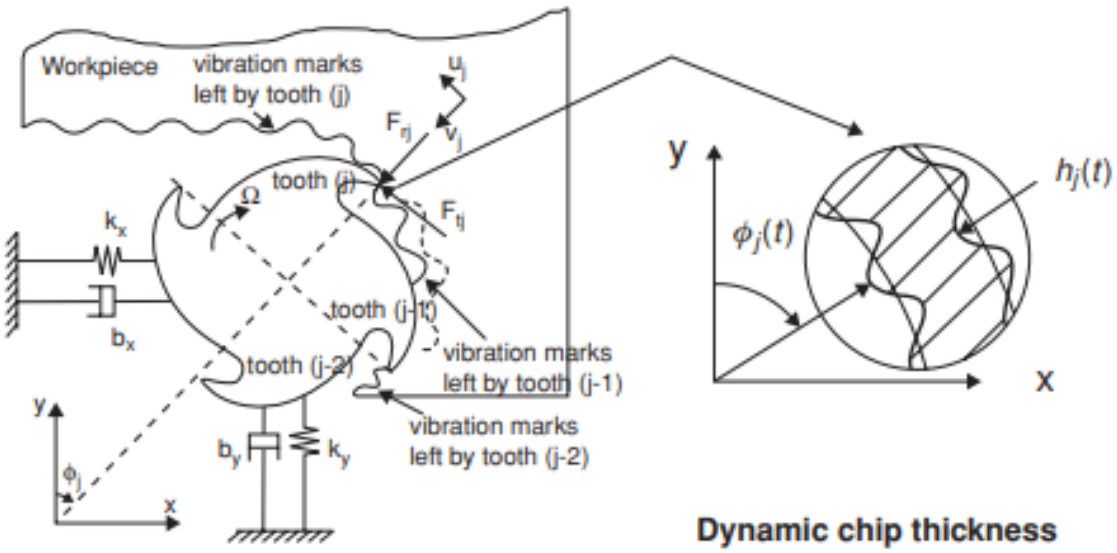

Figure 10.2 DOF milling model

According to Figure 10,the dynamics of milling is modelled by considering the milling cutters to have two orthogonal degrees of freedom in the X and Y directions. Two decoupled differential equations characterize the resulting dynamical system as a combination of mass (m), damping (c), and spring

$$m_x\ddot{x} + c_x\dot{x} + k_x x = F_x$$

$$m_y\ddot{y} + C_y\dot{y} + k_y y = F_y \qquad 15$$

By rearranging the terms by including the damping ratio $\xi = \frac{c}{2\omega m}$, the natural frequency $\omega = \sqrt{\frac{k}{m}}$ and the cutting force in all directions $\bar{F} = \frac{F}{m}$, the equation below is obtained.

$$\begin{Bmatrix}\ddot{x}\\ \ddot{y}\end{Bmatrix} + \begin{bmatrix}2\xi\omega_x & 0\\ 0 & 2\xi\omega_y\end{bmatrix}\begin{Bmatrix}\dot{x}\\ \dot{y}\end{Bmatrix} + \begin{bmatrix}{\omega_x}^2 & 0\\ 0 & {\omega_y}^2\end{bmatrix}\begin{Bmatrix}x\\ y\end{Bmatrix} = \begin{bmatrix}\bar{F}_x\\ \bar{F}_y\end{bmatrix} \qquad 16$$

There are two contributions for chip thickness. The first one is the static part which is due to rigid motion of the tool. The second is the dynamic hip thickness which is due to vibrations of the tool at the present and previous tooth pass.

$$h(\varphi_j) = \left[s_t \sin\varphi_j + \left(v_{j,0} - v_j\right)\right] g(\vartheta_j) \qquad 17$$

where S_t is feed rate per tooth and $v_{j,0}, v_j$ are tool tip dynamic displacements of the previous and actual tooth periods. The engagement of the tool is represented by the unit step function $g(\vartheta_j)$.

$$g(\vartheta_j) = 1, if\ \vartheta_{in} < \vartheta_j < \vartheta_{out}$$

$$g(\vartheta_j) = 0, if\ \vartheta_j < \vartheta_{in}\ or\ \vartheta_j > \vartheta_{out} \qquad 18$$

Where the ϑ_{in} and ϑ_{out} represent the starting and exit immersion angles of the cutter. By combining the equations, the equation below is obtained.

$$h(\varphi_j) = [s_t\, sin\, \varphi_j + (\Delta x\, sin\varphi_j - \Delta y\, cos\varphi_j)]g(\vartheta_j) \qquad 19$$

where $\Delta x = x(t) - x(t-\tau)$ and $\Delta y = y(t) - y(t-\tau)$ are the differences between actual and delayed positions pf the tooth passed along the directions. The delay between two subsequent pass is represented by τ .

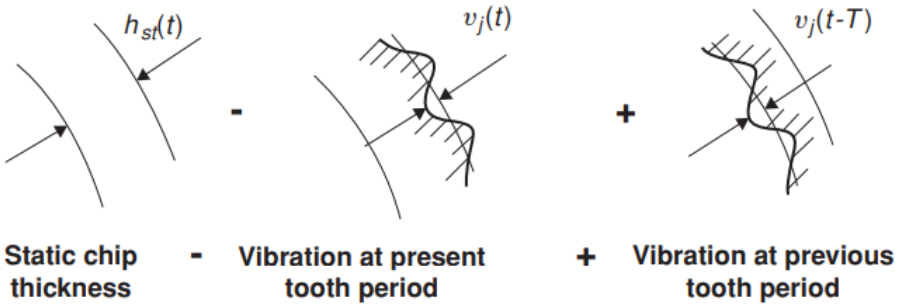

Figure 11.Chip thickness

Then the tangential Ft,j and radial Fr,j cutting forces acting on the j-th tooth are:

$$F_{t,j} = K_t\, a_p h(\varphi_j)$$

$$F_{r,j} = K_r F_{t,j} \qquad 20$$

Where K_t and K_r are cutting coefficients. specific cutting forces are needed to characterize cutting force by means of mathematical models. These coefficients depend on the yield strength of the material, friction between the tool and the workpiece, and tool geometry. The forces are described as the product between

the specific cutting forces and the chip area. Hence, it can be defined as the gain in the regenerative system's closed loop dynamics. The specific cutting forces can be obtained mechanistically by conducting the cutting tests. These cutting coefficients are identified after performing several cutting tests on the machine tool by changing the f_z feed per tooth, the cutting velocity and the depth of cut.

To obtain the cutting forces in the X and Y directions, applying the coordinate transformation

$$F_{x,j} = -F_{t,j}cos\varphi_j - F_{r,j}sin\varphi_j$$

$$F_{y,j} = F_{t,j}sin\varphi_j - F_{r,j}cos\varphi_j \quad (21)$$

The total cutting forces acting on a tool are the sum of cutting forces acting on each tooth in the cut.

$$F_x = \sum_{j=0}^{N-1} F_{x,j}$$

$$F_y = \sum_{j=0}^{N-1} F_{y,j} \quad (22)$$

Hence, due to the delayed terms of the chip thickness expression, the dynamical system is now described by time varying delay differential equations.

The regenerative forces can be written by discarding the static chip contribution as

$$\begin{bmatrix} F_{x,r} \\ F_{y,r} \end{bmatrix} = \frac{1}{2} K_t \, a_p \, A_D(t) \begin{bmatrix} \Delta x \\ \Delta y \end{bmatrix} \quad (23)$$

Where $A_D(t)$ is built as

$$A_D(t) = \begin{bmatrix} a_{xx} & a_{xy} \\ a_{yx} & a_{yy} \end{bmatrix} \quad (24)$$

$$a_{xx} = \sum_{j=1}^{N-1} -g(\vartheta_j)\left[sin\,2\,\varphi_j + K_r\left(1 - cos2\varphi_j(t)\right)\right] \quad (25)$$

$$a_{xy} = \sum_{j=1}^{N-1} -g(\vartheta_j)[(1 + \cos 2\,\varphi_j) + K_r \sin 2\,\varphi_j(t)\,]$$

$$a_{yx} = \sum_{j=1}^{N-1} g(\vartheta_j)[(1 - \cos 2\,\varphi_j) - K_r \sin 2\,\varphi_j(t)\,]$$

$$a_{yy} = \sum_{j=1}^{N-1} -g(\vartheta_j)[\sin 2\,\varphi_j - K_r(1 + cos2\varphi_j(t))\,]$$

This is the cutting force model with the time varying directional dynamics milling force coefficients.

$$\begin{Bmatrix}\ddot{x}\\ \ddot{y}\end{Bmatrix} + \begin{bmatrix}2\xi\omega_x & 0\\ 0 & 2\xi\omega_y\end{bmatrix}\begin{Bmatrix}\dot{x}\\ \dot{y}\end{Bmatrix} + \begin{bmatrix}{\omega_x}^2 & 0\\ 0 & {\omega_y}^2\end{bmatrix}\begin{Bmatrix}x\\ y\end{Bmatrix} = \begin{bmatrix}F_{x,nom}\\ F_{y,nom}\end{bmatrix} + \frac{1}{2}K_t\, a_p\; A_D(t)\begin{Bmatrix}x(t) - x(t-\tau)\\ y(t) - y(t-\tau\end{Bmatrix} \quad 26$$

And by rearranging the equation,

$$\begin{Bmatrix}\ddot{x}\\ \ddot{y}\end{Bmatrix} + \begin{bmatrix}2\xi\omega_x & 0\\ 0 & 2\xi\omega_y\end{bmatrix}\begin{Bmatrix}\dot{x}\\ \dot{y}\end{Bmatrix} + \begin{bmatrix}{\omega_x}^2 - \frac{1}{2}K_t\, a_p\, a_{xx} & -\frac{1}{2}K_t\, a_p\, a_{xy}\\ -\frac{1}{2}K_t\, a_p\, a_{yx} & {\omega_y}^2 - \frac{1}{2}K_t\, a_p\, a_{yy}\end{bmatrix}\begin{Bmatrix}x\\ y\end{Bmatrix} + \begin{bmatrix}\frac{1}{2}K_t\, a_p\, a_{xx} & \frac{1}{2}K_t\, a_p\, a_{xy}\\ \frac{1}{2}K_t\, a_p\, a_{yx} & \frac{1}{2}K_t\, a_p\, a_{yy}\end{bmatrix}\begin{Bmatrix}x(t-\tau)\\ y(t-\tau)\end{Bmatrix} = \begin{bmatrix}F_{x,nom}\\ F_{y,nom}\end{bmatrix} \quad 27$$

It is common to show obtained system models and equations in state space representation as below

$$\dot{x}(t) = Ax(t) + Bu(t)$$
$$y(t) = Cx(t) + Du(t) \quad 28$$

Before combining the milling equations with the state-space representation, it must be recalled that

$$u(t) = F_{nom}(t) + F_r(t) = F_{nom}(t) + \frac{1}{2}K_t\, a_p\; A_D(t)\begin{Bmatrix}x_{tooltip}(t) - x_{tooltip}(t-\tau)\\ y_{tooltip}(t) - y_{tooltip}(t-\tau)\end{Bmatrix}$$

$$y(t) = Cx(t) \quad 29$$

By combining with the state -space representation

$$\dot{x}(t) = Ax(t) + BF_{nom}(t) + \frac{1}{2}BK_t\, a_p\;\; A_D(t)Cx(t) - \frac{1}{2}BK_t\, a_p\;\; A_D(t)Cx(t-\tau)$$

$$y(t) = Cx(t) \qquad 30$$

Organization of the equations must be done carefully for not allowing any misunderstanding. After organizing the equations new matrix $A(t) = A + \frac{1}{2}Ba_pKtA_D(t)C$ and $B(t) = -\frac{1}{2}BK_t\, a_p\;\; A_D(t)C$, the general state space representation can be shown as

$$\dot{x}(t) = A(t)x(t) + B(t)x(t-\tau) + BF_{nom}(t)$$

$$y(t) = Cx(t) \qquad 31$$

It must be carefully noted the difference between B and $B(t)$. The time varying nature of $B(t)$ comes from the time dependent directional force coefficients not from time dependent input values. Same explanation is valid for matrix $A(t)$ where the time dependence comes from matrix $A_D(t)$ not form machine dynamics change.

2.3.2 Linear Time-Periodic System

Milling dynamics for LTP systems will be introduced according to figure below by introducing the time-variant behavior of stiffness. Because in this thesis, the system's stiffness is varied periodically by changing the length of the tool holder bar. By introducing stiffness variation to the 2-DOF milling system,

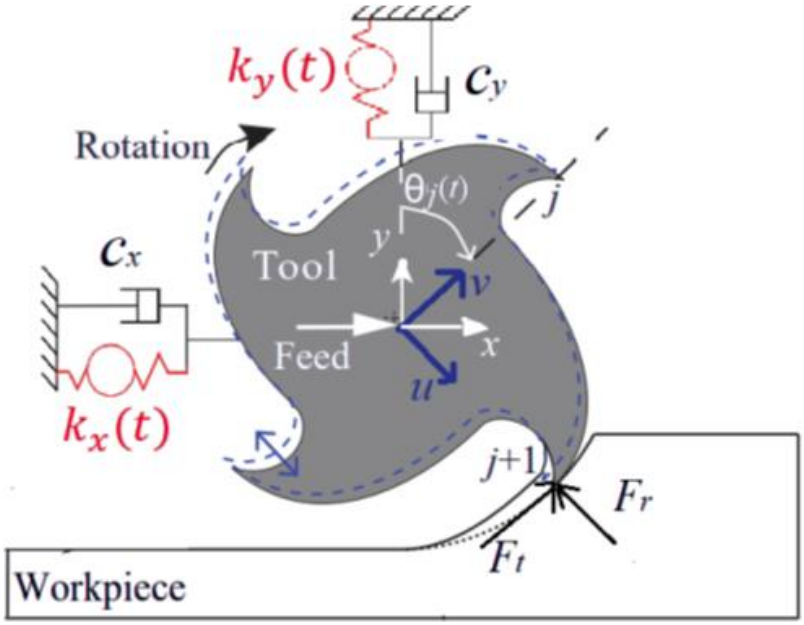

Figure 12. Milling model by time-varying stiffness

For using the same notation with the reference paper [12], $[x\ y] = q$ transformation will be used. Therefore, the equation in 2-DOF milling will become as

$$\{\ddot{q(t)}\} + \begin{bmatrix} 2\xi_x\omega_{nx} & 0 \\ 0 & 2\xi_y\omega_{ny} \end{bmatrix}\{\dot{q(t)}\} + \begin{bmatrix} {\omega_{nx}}^2 & 0 \\ 0 & {\omega_{ny}}^2 \end{bmatrix}\{q(t)\}$$
$$= \frac{1}{2}K_t\, a_p \begin{bmatrix} a_{xx} & a_{xy} \\ a_{yx} & a_{yy} \end{bmatrix} \begin{bmatrix} \frac{1}{m_x} & 0 \\ 0 & \frac{1}{m_y} \end{bmatrix} \begin{Bmatrix} q(t-\tau) \\ q(t-\tau) \end{Bmatrix} \qquad 32$$

Considering the 2 DOF stiffness variation model as in the figure, variation of stiffness around the natural frequency with a function $f_i(t)$ will be involved to the equation.

$$\{\ddot{q}(t)\} + \begin{bmatrix} 2\xi_x\omega_{nx} & 0 \\ 0 & 2\xi_y\omega_{ny} \end{bmatrix}\{\dot{q(t)}\} + \begin{bmatrix} {\omega_{nx}}^2\big(1+f_x(t)\big) & 0 \\ 0 & {\omega_{ny}}^2\Big(1+f_y(t)\Big) \end{bmatrix}\{q(t)\}$$
$$= \frac{1}{2}K_t\, a_p \begin{bmatrix} a_{xx} & a_{xy} \\ a_{yx} & a_{yy} \end{bmatrix} \begin{bmatrix} \frac{1}{m_x} & 0 \\ 0 & \frac{1}{m_y} \end{bmatrix} \begin{Bmatrix} q(t-\tau) \\ q(t-\tau) \end{Bmatrix} \qquad 33$$

This equation obtained will be used to tell Harmonics Transfer function concept in the stability analysis part as in [12].

2.4 Stability

The stability assessment can be divided into two as out-of-process and in-process methods. The out-of-process methods predict the cutting process's stability boundary and allow for choice of suitable parameters for the chatter-free cutting process. These stability boundaries are called Stability Lobe Diagrams (SLD). These diagrams must be identified before the process. However, in-process methods detect chatter during the machining operation and parameters are changed to have a stable cut.

2.4.1Out-of Process (Chatter Prediction)

This part explains how to avoid self-excited vibration without modifying the characteristics of the system by emphasizing for both LTI and LTP systems. Optimal cutting parameters are chosen by searching for the stable regions with maximum material removal rate.

2.4.1.1Linear Time-Invariant System

Reliable prediction of the stability of the milling process has a crucial importance. The SLD are estimated for systems with LTI or LTP dynamics and known parameters. However, the uncertainty and varying nature of the system dynamics and parameters subvert this estimation process. For instance, machine tool-workpiece dynamic is always an uncertain parameter and usually obtained by impact test. This test is simple but full of uncertainties. Also, the cutting coefficient K_t is an estimation. These parameters can also vary during the process. This change results in unreliable SLD. Uncertainties in predicting the SLD can cause many disastrous results. As mentioned earlier, the stability lobe diagrams can be estimate by for inputs as in Figure 13.

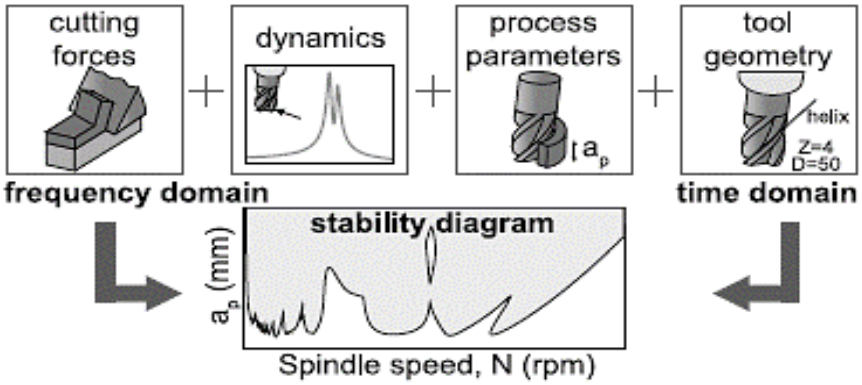

Figure 13. SLD and SLD affecting factors

For chatter prediction, the regenerative effect in milling is modelled by a delay-differential equation as discussed earlier. The boundary between unstable (with chatter) and stable (without chatter) can be anticipated. For separating these regions, Stability Lobe Diagrams (SLD) can be useful. The SLD shows the critical depth of cut against spindle speed and these graphs can be useful for optimizing the machining process. This process can be carried out in time domain (i.e., semi-discretization, full discretization etc.) or frequency domain.

Time domain methods chatter prediction methods are based on Delayed Differential Equation Theory. Insperger et al. developed the Semi discretization method [13] which consist of performing stability analysis by splitting time into equally spaced time intervals. $A(t)\ and\ B(t)$ are approximated as constant matrices by discretizing the delayed term $x(t-\tau)$. The ability to predict SLD of Semi Discretization method is high for high number of intervals. In Full discretization method the term x(t) is also discretized [14] and maintains a higher rate of prediction efficiency. The accuracy is higher compared to SD method. However, they all suffer from long processing time.

In frequency domain analysis, Zero-Order approximation (ZOA) method was proposed by Altintas and Budak [11].This method considers an average coefficient of Fourier series to expand time-dependent periodic directional coefficients matrix $A_D(t)$.The number of harmonics r of the tooth passing frequency to be considered for an accurate reconstruction of $A_D(t)$.

$$A_D(t) = \sum_{r=-\infty}^{\infty} A_r e^{irwt}$$

$$A_r = \frac{1}{T}\int_0^T A(t)e^{-irwt}dt$$

$$A_{r,0} = \int_0^T A(t)dt \qquad 34$$

Since $A_{r,0}$ is valid only when the tooth is engaged, it is equal to the average value at the cutter pitch angle $\varphi_p = \frac{2\pi}{N}$. According to this new directional force coefficient matrix can be written as

$$A_{r,0} = \int_{\vartheta_{in}}^{\vartheta_{out}} A(\vartheta)d\vartheta = \frac{N}{2\pi}\begin{bmatrix} a_{xx} & a_{xy} \\ a_{yx} & a_{yy} \end{bmatrix} \qquad 35$$

The method was computationally efficient but inappropriate for low immersion cutting where number of cutting edges are relatively small [5,6]. Consequently, there is either only one edge in contact or no contact between tool and workpiece for a relatively short period of time [16].This is because low immersion cutting is used while cutting hard materials and cutting force varies much and it is not appropriate to take average chip thickness i.e. autonomous approximation. Merdol and Altintas proposed a solution to overcome this limitation by higher-order harmonics .They presented the multi-frequency solution [17]. Multi frequency solution can give more accurate results. Although computation time increases, it also doesn't take non-linearities during milling process as in time domain methods.

Gradisek et al. made a research for low radial immersion milling to compare ZOA and SD methods [18]. The most prominent difference was as additional set of lobes corresponding to a new type of instability called period doubling bifurcation (flip bifurcation). SD method was able to predict this type of instability compared to ZOA solution. They also showed that in the case of decreasing the radial immersion, the gap between predicted SLD was increasing.

2.4.1.2 Linear Time-Periodic System

As stated earlier, the complex exponential signals are not enough to describe input-output relationship for LTP systems. The output will be the sum of three complex exponentials in the case of applying $1 + a_{sv}sin\omega_p t$ where ω_p is the pumping frequency.

$$y(t) = e^{st} + a_{sv}e^{(s+i\omega_p)t} + a_{sv}e^{(s-i\omega_p)t} \quad 36$$

It is clear to see that the output is modulated by the harmonics of the pumping frequency. By using the equation 10 as the base form of HTF, the independency of each element can be shown as

$$\begin{pmatrix} \vdots \\ Y_{-1} \\ Y_0 \\ Y_1 \\ \vdots \end{pmatrix} = \begin{bmatrix} \ddots & \vdots & \vdots & \vdots & \ddots \\ \cdots & H_{-1,-1}(s) & H_{-1,0}(s) & H_{-1,1}(s) & \cdots \\ \cdots & H_{0,-1}(s) & H_{0,0}(s) & H_{0,1}(s) & \cdots \\ \cdots & H_{1,-1}(s) & H_{1,0}(s) & H_{1,1}(s) & \cdots \\ \ddots & \vdots & \vdots & \vdots & \ddots \end{bmatrix} \begin{pmatrix} \vdots \\ U_{-1} \\ U_0 \\ U_1 \\ \vdots \end{pmatrix} \quad 37$$

Since the HTF is also known as Frequency-Lifted Transfer Operator, the equation above can be written as

$$\begin{pmatrix} \vdots \\ Y_{-1} \\ Y_0 \\ Y_1 \\ \vdots \end{pmatrix} = \begin{bmatrix} \ddots & \vdots & \vdots & \vdots & \ddots \\ \cdots & H_0(s-i\omega_p) & H_{-1}(s) & H_{-2}(s+i\omega_p) & \cdots \\ \cdots & H_1(s-i\omega_p) & H_0(s) & H_{-1}(s+i\omega_p) & \cdots \\ \cdots & H_2(s-i\omega_p) & H_1(s) & H_0(s+i\omega_p) & \cdots \\ \ddots & \vdots & \vdots & \vdots & \ddots \end{bmatrix} \begin{pmatrix} \vdots \\ U_{-1} \\ U_0 \\ U_1 \\ \vdots \end{pmatrix} \quad 38$$

The main diagonal of the matrix links the input harmonics with output harmonics. The out-of-diagonal terms link the harmonics of the input with harmonics of the output at different frequencies which represent the characteristics of LTP systems.

Since assessing the stability is the main aim in this chapter, the methods used for solving the harmonic transfer functions will be described. In the study [12] , the authors compared the results of zero-order harmonic solution and harmonic solution.

The harmonic solution is derived with applying EMP for the force, the state and the Fourier transformation of the $A_D(t)$ matrix at the pumping frequency.

$$F(t) = \sum_{n=-\infty}^{\infty} P_n e^{(s+in\omega_p)t}$$

$$q(t) - q(t-\tau) = \sum_{m=-\infty}^{\infty} Q_m e^{(s+im\omega_p)t}\left(1 - e^{-(s+im\omega_p)\tau}\right)$$

$$A_D(t) = \sum_{-\infty}^{\infty} \Lambda_{n-m} Q_m \left(1 - e^{-(s+im\omega_p)\tau}\right) e^{(s+im\omega_p)t} \quad 39$$

By substituting these equations into the dynamic milling force equation,

$$\sum_{-\infty}^{\infty} P_n e^{(s+in\omega_p)t} = \frac{1}{2} K_t\, a_p \sum_{n=-\infty}^{\infty}\sum_{m=-\infty}^{\infty}\sum_{l=-\infty}^{\infty} \Lambda_{n-m} H_{l-m}\left(s - il\omega_p\right) P_l\left(1 - e^{-(s+im\omega_p)\tau}\right) e^{(s+im\omega_p)t} \quad 40$$

The harmonic balance equation leads to a set-in term of the following equation:

$$P_n = \frac{1}{2} K_t\, a_p \sum_{m=-\infty}^{\infty}\sum_{l=-\infty}^{\infty} \Lambda_{n-m} H_{l-m}\left(s - il\omega_p\right) P_l\left(1 - e^{-(s+im\omega_p)\tau}\right) \quad 41$$

By expanding the matrices at the stability limit

$$\begin{pmatrix} \vdots \\ P_{-1} \\ P_0 \\ P_1 \\ \vdots \end{pmatrix} = \frac{1}{2} K_t\, a_p \left(\begin{bmatrix} \ddots & \vdots & \vdots & \vdots & \ddots \\ \cdots & I & 0 & 0 & \cdots \\ \cdots & 0 & I & 0 & \cdots \\ \cdots & 0 & 0 & I & \cdots \\ \ddots & \vdots & \vdots & \vdots & \ddots \end{bmatrix} - \begin{bmatrix} \ddots & \vdots & \vdots & \vdots & \ddots \\ \cdots & Ie^{-i(\omega_c-\omega_p)\tau} & 0 & 0 & \cdots \\ \cdots & 0 & Ie^{-i(\omega_c)\tau} & 0 & \cdots \\ \cdots & 0 & 0 & Ie^{-i(\omega_c+\omega_p)\tau} & \cdots \\ \ddots & \vdots & \vdots & \vdots & \ddots \end{bmatrix} \right)$$

$$= \begin{bmatrix} \ddots & \vdots & \vdots & \vdots & \ddots \\ \cdots & \Lambda_0 & \Lambda_{-1} & \Lambda_{-2} & \cdots \\ \cdots & \Lambda_1 & \Lambda_0 & \Lambda_{-1} & \cdots \\ \cdots & \Lambda_2 & \Lambda_1 & \Lambda_0 & \cdots \\ \ddots & \vdots & \vdots & \vdots & \ddots \end{bmatrix} \begin{bmatrix} \ddots & \vdots & \vdots & \vdots & \ddots \\ \cdots & H_0(i\omega_c - i\omega_p) & H_{-1}(i\omega_c) & H_{-2}(i\omega_c + i\omega_p) & \cdots \\ \cdots & H_1(i\omega_c - i\omega_p) & H_0(i\omega_c) & H_{-1}(i\omega_c + i\omega_p) & \cdots \\ \cdots & H_2(i\omega_c - i\omega_p) & H_1(i\omega_c) & H_0(i\omega_c + i\omega_p) & \cdots \\ \ddots & \vdots & \vdots & \vdots & \ddots \end{bmatrix} \begin{pmatrix} \vdots \\ P_{-1} \\ P_0 \\ P_1 \\ \vdots \end{pmatrix} \quad 42$$

The expanded matrices in the above equation have infinite dimension. It is required to truncate the harmonics for creating the stability map. As will be explained in Chapter 3, the experiments conducted in our work, has constant stiffness variation and high radial depth of cut. In [11], Altintas stated that the directional matrix $A_D(t)$ can be assumed as $A_{D,0}$ in the case of high radial depth. $A_{D,0}$ is the average value of the directional matrix and gives a good approximation of SLD. By this assumption the dimension is reduced and the harmonics of the HTF are considered since the periodicity is only due to harmonic transfer function. ($\omega_p = \omega_{sv}$)

$$\begin{pmatrix} \vdots \\ P_{-1} \\ P_0 \\ P_1 \\ \vdots \end{pmatrix} = \frac{1}{2} K_t\, a_p \left(\begin{bmatrix} \ddots & \vdots & \vdots & \vdots & \ddots \\ \cdots & I & 0 & 0 & \cdots \\ \cdots & 0 & I & 0 & \cdots \\ \cdots & 0 & 0 & I & \cdots \\ \ddots & \vdots & \vdots & \vdots & \ddots \end{bmatrix} - \begin{bmatrix} \ddots & \vdots & \vdots & \vdots & \ddots \\ \cdots & Ie^{-i(\omega_c-\omega_p)\tau} & 0 & 0 & \cdots \\ \cdots & 0 & Ie^{-i(\omega_c)\tau} & 0 & \cdots \\ \cdots & 0 & 0 & Ie^{-i(\omega_c+\omega_p)\tau} & \cdots \\ \ddots & \vdots & \vdots & \vdots & \ddots \end{bmatrix} \right)$$

$$= \begin{bmatrix} \ddots & \vdots & \vdots & \vdots & \ddots \\ \cdots & \Lambda_0 & \Lambda_0 & \Lambda_0 & \cdots \\ \cdots & \Lambda_0 & \Lambda_0 & \Lambda_0 & \cdots \\ \cdots & \Lambda_0 & \Lambda_0 & \Lambda_0 & \cdots \\ \ddots & \vdots & \vdots & \vdots & \ddots \end{bmatrix} \begin{bmatrix} \ddots & \vdots & \vdots & \vdots & \ddots \\ \cdots & H_0(i\omega_c - i\omega_{sv}) & H_{-1}(i\omega_c) & H_{-2}(i\omega_c + i\omega_{sv}) & \cdots \\ \cdots & H_1(i\omega_c - i\omega_{sv}) & H_0(i\omega_c) & H_{-1}(i\omega_c + i\omega_{sv}) & \cdots \\ \cdots & H_2(i\omega_c - i\omega_{sv}) & H_1(i\omega_c) & H_0(i\omega_c + i\omega_{sv}) & \cdots \\ \ddots & \vdots & \vdots & \vdots & \ddots \end{bmatrix} \begin{pmatrix} \vdots \\ P_{-1} \\ P_0 \\ P_1 \\ \vdots \end{pmatrix} \quad 43$$

After obtaining this equation above, the stability can be determined by finding the

roots of equation. The formulation depends on the dynamical properties and directional matrix approximation. Since in this study LTP system is considered, the roots are non-trivial solutions. The root finding problem can be written as

$$det\left(I-\frac{1}{2}K_t\,a_p\left(A_{D,T}-A_{D,T}\varepsilon\right)\widehat{H}\right)=D\left(\,a_p,\Omega,\omega_c\right)=0 \qquad 44$$

where $A_{D,T}$ is the Toeplitz transform of directional matrix A_D and $\varepsilon = Ie^{-i(\omega_c+m\omega_p)t}$ at the stability limit. The solution is obtained by applying Multi-Dimensional Bisection Method. This needs the desired spindle speed range, expected depth of cut and chatter frequency range definition. Choosing the chatter frequency range has a critical importance and good results can be obtained by defining a range around natural frequency $\left[\omega_n-\frac{\omega_p}{2},\omega_n+\frac{\omega_p}{2}\right]$. By implying the same modal parameters and cutting conditions, the convergence of SLD with different number of harmonics are compared and this graph is essential for understanding the importance of the truncation of harmonics in the case of LTP system.

A possible solution of the HTF has been presented in this part. As can be seen, complex and burden mathematical equations are required to be solved. That is one of the biggest motivations of developing online chatter detection methods which are presented in the next chapter.

2.4.2 In Process-Chatter Detection

The chatter prediction by estimation of the stability lobes is off-line approach to prevent unstable cutting. This approach needs complete machine dynamics analysis and it is not easy to be done by the users. Since off-line approach needs deep knowledge of process, online chatter detection has become very important due to the development of information technology and advanced sensors. Appropriate sensors must be applied to acquire the useful data. After acquiring the signals, the meaningful features must be extracted from raw signals and chatter identification model must be built to detect chatter. The last step is to find a chatter suppression technique.

2.4.2.1Data Acquisition

Data acquisition techniques can be categorized by two methods which are indirect and direct ones. The direct methods include laser beams, electrical resistance, radioactive isotopes and the use of camera. Direct measurements have high level accuracy. Although they give reliable results, there are practical application limitations during machining and the use of cutting fluid. This is one of the reasons why these methods are only applicable in the laboratory environment. Indirect methods are more appropriate for practical applications since they are less complex. These methods are less accurate compared to direct methods but provides continuous monitoring info via sensing devices.

Motor power and current signals are the components which produce the forces to cut material [19]–[21]. These measurements give information about cutting tool condition. The motor related parameters are obtained far from cutting area. Therefore, measurement process is not affected by cutting environment. There is a linear relation between measured motor current or power and output force or torque. The drawback of this method sensitivity might not be enough for quality information.

The cutting force monitoring [22], [23] is necessary for the validation of the analytical process to detect tool wearing and life. This method of indirect measurement is sensitive to cutting condition and gives rapid response. Two main types of force and torque sensors are piezoelectric and strain-based sensors. Piezoelectric based sensors are preferred when the flexibility is required. Strain gauge force transducers offer high frequency response.

Acoustic emission (AE) sensors have found a wide area of application in chatter detection. These sensors are subjected to multiple effects as installation location and operation mode. Also, feature extraction by using acoustic emission sensors are very challenging since it is very sensitive to environmental noise [24].

Sound signal sensors can provide important information about machining condition[25]–[27]. Many research proved that it can be helpful to identify chatter. A microphone is placed closed to the cutting area which limits the filtering effects

between process and sensor. These sensors have high sensitivity to low cutting force and low radial immersion cutting conditions.

Vibration sensors have been used due to their rapid response to chatter occurrence [28], [29].Measurement can be performed by using accelerometers which determine the dynamic acceleration on the tool as a voltage. The biggest advantage is the linearity between a wide frequency range. They use the piezoelectric method to measure acceleration The energy of vibration increases when chatter occurs. They can be assembled to the spindle housing and features can be extracted with the use of advanced signal processing techniques.

2.4.2.2 Feature Extraction

Mainly, the feature extraction of raw data can be classified in three main categories. There are time-domain, frequency domain and time-frequency domain.

2.4.2.2.1 Time Domain Methods

Time domain features can describe the signal and maintain as much as information about process. These features are obtained by the calculation of statistical features or statistical moments. Most common features are root mean square (RMS), variance, standard deviation, kurtosis, skewness, peak-to-peak values, peak-to-valley amplitude, crest factor and ratio of the signals for process monitoring. The RMS indicator is a standard measure that returns an evaluation in amplitude directly related to the energy content of the signal. The kurtosis is defined as the fourth statistical moment divided by the square of the second statistical moment as in Table 1. Skewness measures the relative energy above and below the mean value. Crest factor is the ratio between peak value and the RMS value. For example, standard deviation of the force calculated and used as a chatter indicator for drilling in [30] .In [31], a synthetic criterion was developed by combining standard deviation and auto-correlation function for chatter detection. Kurtosis distribution of the acquired vibration signal used as a chatter indicator for grinding process in [32].

Table 1. Statistical features' formulas

N.	Name	Outputs	Units
1	RMS[a]	$\sqrt{\frac{1}{N}\sum_{i=1}^{n}\lvert X_n\rvert^2}$	m/s^2
2	Kurtosis	$\frac{\frac{1}{N}\sum_{i=1}^{n}(X_i-\bar{X})^4}{\left(\frac{1}{N}\sum_{i=1}^{n}(X_i-\bar{X})^2\right)^2}$	-
3	Skewness	$\frac{\frac{1}{N}\sum_{i=1}^{n}(X_i-\bar{X})^3}{\left(\frac{1}{N}\sum_{i=1}^{n}(X_i-\bar{X})^2\right)^3}$	-
4	Peak to peak	$\lvert X_{max}-X_{min}\rvert$	m/s^2
5	Peak to RMS	$\frac{\lvert\lvert X\rvert\rvert_\infty}{\sqrt{\frac{1}{N}\cdot\lvert X_n\rvert^2}}$	-

There are also some methods based on time series modelling as auto-regressive, moving average and auto-regressive-moving-average. In [33], a nonlinear time series modelling was adopted to represent time varying dynamics of the cutting process. However, these methods were not further investigated in this research activity.

2.4.2.2.2 Frequency Domain Methods

It is well known that chatter causes frequency redistribution. Feature extraction on the frequency domain is carried through windowed Fourier transform. It mustn't be forgotten that sufficient amount of data is required for frequency domain analysis. This approach requires high sampling rate to eliminate aliasing or increasing the window length for obtaining enough data to have enough resolution. With Fourier Transform the sine waves are represented in the frequency domain with amplitude and phase. One of the most common and practical methods is Fast Fourier Transform. The features obtained in the frequency spectrum may be inspected by the statistical methods as variance, skewness and kurtosis. Hynynen et al. [26] used the coherence function of the acceleration and audio signal to early detection of chatter. They validated that the method was sensitive to chatter onset. After obtaining FFT, the power spectral density can also be calculated according to the values. For example, in [25], the PSD of the audio signal was calculated to assess the stability of the process.

In the frequency domain methods, it also has a crucial importance to mention used indicators. One must recall that the chatter properties can be separated by distinguishing synchronous and asynchronous frequency components. Synchronous part will include tooth passing frequencies while the other spectral components can be described as chatter related components. In this sense, relative maximum synchronous excitation value (SEV), relative SEV, Absolute SEV, relative maximum SEV are developed and used.

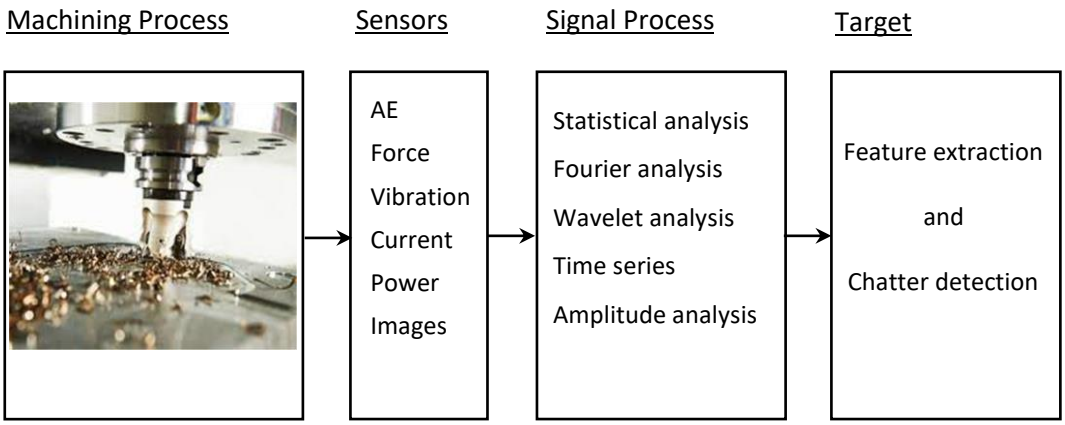

Figure 14. In-process chatter detection strategy

2.4.2.2.3 Time-Frequency Methods

Time-frequency technique are widely sued in feature extraction. These methods are Short-Time Fourier Transform (STFT), wavelet-based methods, empirical mode decomposition based (EMD) methods and variational mode decomposition (VMD) based methods These advanced signal processing methods decompose the chatter signal into some components/modes corresponding to different frequency bands. The decomposition components/modes, including rich chatter information, can serve to highlight and extract the chatter features.

STFT uses a sliding window to characterize the change of frequency components at different time intervals. Spectral coefficients are calculated for this data and then window is moved to another position. It can also be described as Fourier transform repetition for consecutive time intervals [34]. The major drawback of this method is both frequency resolution and time localization cannot be high meanwhile.

Wavelet Transform was developed in order to remove drawbacks of the STFT. This method uses different window lengths for different frequencies. High frequencies are analyzed with narrower windows are used for better time localization while for lower frequencies wider windows are used for better frequency resolution. Hence, it can give more information for different frequency bands. The discrete Wavelet Transform gives approximation coefficients and wavelet coefficients by convolution of the signal. Wavelet coefficients are handled as There is another type of wavelet method which is called Wavelet Packet Decomposition (WPT). This method creates more frequency bands. Therefore, it can provide more useful spectral features. For Wavelet based methods there is a mother wavelet which decomposes the signal by shifting and scaling. The drawback of WPT is the higher computational cost compared to DWT. There are many studies in process monitoring with wavelet based methods [35]–[38]. The comparison results showed that WT based methods gave better results with force signals while the FFT was better for vibration signals. Also in a recent study [39], the authors compared the wavelet based method and FFT and for real-time chatter detection and showed that FFT gives much rapid response.

Empirical Mode Decomposition (EMD) is a time-adaptive signal decomposition method. The signal is decomposed to the almost orthogonal mono-component Intrinsic Mode Functions (IMF). After obtaining the IMFs, HHT is applied. This method examines the instantaneous frequency and generates an effective Time-Frequency which is called Hilbert spectrum. This method is especially designed for non-stationary and non-linear signals. It can be assessed more like an empirical approach instead of theoretical approach [40].HHT doesn't have frequency resolution or time localization concept and gives a uniform high frequency resolution in full frequency range. There are also combined methods which uses wavelet and HHT. Cao et al. [28] decomposed the acceleration signal to reconstruct the signal. Then HHT is applied to the reconstructed signal to obtain energy distribution of the signal. The state of the cutting process was decided according to Hilbert spectrum analysis. Although HHT is a self-adaptive method which makes it practically applicable, since it is a EMD based method, it is sensitive to noise.

Variational Mode Decomposition is a non-recursive method and decomposes the input signal into different amplitude and frequency modulated wave such that jointly

they reconstruct the original signal which outperforms the EMD in robustness. A method which detects chatter by combining VMD and energy entropy was proposed [41]. The results showed that sensitivity to chatter occurrence was improved. The drawback is this method is the required number of signal components as a priori parameter [41].

2.5 Chatter Suppression Techniques

In milling process, the chatter avoidance or suppression technique must be applied after chatter prediction or detection. This is a challenging process. These methods can be classified by passive and active methods. The passive methods aim to enlarge the SLD which can be distinguished as out of process and called as chatter avoidance techniques. Although, there are many methods used to avoid chatter by changing the SLD of the process [5] , active suppression techniques used in the literature are introduced in this part.

Active chatter suppression methods monitor the dynamic state of the machine tool system and change the system to a better position if it is possible. The dynamics of the system are modified, and stable zone is expanded thanks to this system modification. In [42] , the chatter is suppressed by using an active electrostatic and piezoelectric spindle bearing support. In other words, they change the response function of the system. There are many studies which used the spindle speed variation strategy to suppress chatter [43], [44]. However, they weren't satisfactory for real-time application. In [45] , the authors aimed to change the stiffness of the boring bar by varying the strength of the applied magnetic field of magnetorheological fluid. Wang et al. [46] studied on suppressing the chatter with changing the stiffness with piezoelectric stack actuators. The authors studied on changing the stiffness of the bar by changing the length periodically which is the base of this project [12] .

3 Experimental Setup

In this part, the machine and the accelerometer used will be introduced. The stiffness variation control strategy has been applied to machine tool produced by PAMA S.p.A. model VERTIRAM 2000 GT. It is a vertical movable gantry machining center which is designed to process heavy components. VERTIRAM CNC machining centers can be customized with a wide range of turning tables with loading capacity from 25 to 300 tons. Different heads for customized solutions, tool magazines and other accessories can be implemented.

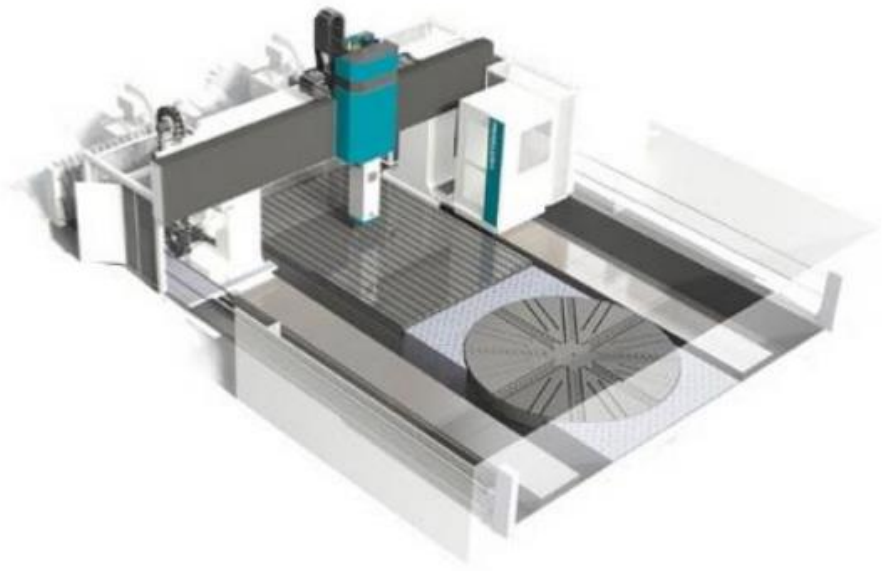

Figure 15. PAMA VERTIRAM 2000 GT machining center

Table 2. Machining center technical details

WORKING AREA		
Clearance between columns	mm	3000 – 10100
Clearance under spindle (AL200)	mm	1700 – 5500
X axis (gantry)	mm	4000 – 6000
	mm	+N x 1000
Y axis (headstock)	mm	3000 – 11600
Z axis (ram)	mm	1300 – 2500
W axis (cross-rail – option)	mm	1100 – 3600
TABLE (FLOOR PLATES)		
Table (floor plates) width	mm	2000 – 9000
HEADSTOCK		
Ram section	mm	500 x 500 – 590 x 590
Max. spindle speed	rpm	3000 – 7000
Spindle gear ranges		Direct Drive / 4
Max spindle power (S1)	kW	45 – 103
Max spindle torque (S1)	Nm	800 – 10730
AXES FEED RATES		
X, Y, Z, V rapid traverse/feed rate	mm/min	up to 30000
W axis rapid traverse/feed rate	mm/min	3000

The Z-axis and W-axis which are related to the ram and boring bar, respectively. These axes are coaxial with the spindle. It must be noted that different combinations of Z+W results in different stiffness values as can be seen in Figure 16. By changing this combination without changing the tool tip position, the machine dynamics are changed, and the suppression of chatter is aimed.

The accelerometer is assembled to the front face of the ram which is the closest fixed part to the tool. The used accelerometer has sensitivity of 10 mV/g. The signals are acquired through National Instruments Ethernet cDaq and the NI-9234 module. The data are gathered through a software developed by Consorzio MUSP.

The cutting tool diameter is 80 mm and has 2 teeth in all experiments. The cutting strategy is to try five different spindle speeds with SV on and off.

Figure 16.The axes where stiffness variation realized

4 Methods

The methods used for detecting the spindle speed and status of modulation strategy and chatter indicator are explained step by step in this part.

4.1 Pre-Analysis

The experiments are conducted with different depth of cut, spindle speed, different machine positions for both stiffness modulation on and off. Acquired data provides information about accelerometer values in three directions (cx,cy,cz), sampling frequency (fs), time vector (time) and the spindle speeds used (omega) during the experiment. This doesn't provide the knowledge about the change of conditions such as when did the spindle speed change or the modulation was active or not as in Figure 17. This information has a high importance to be able to understand chatter related components. In other words, if the cut is performed a specific spindle speed Ω , it is expected to see excitations on the tooth passing frequency and its harmonics $tpf(Hz) = \frac{\Omega N}{60}$. Also, if stiffness modulation is performed it is expected to observe sidebands around the system frequency and its harmonics. Therefore, the data to be processed must provide this information. Otherwise, one needs to check the frequency spectrum of interested window and see the dominant frequencies. As a matter of fact, one must repeat this until detecting the change of inputs. Conducting this analysis manually is time consuming and decision depends on a subjective interpretation. It means that it might not be repetitive. Therefore, plotting the data according to the input change as a pre-analysis before creating a chatter detection algorithm. For this purpose, an automatic detection algorithm was developed. It consists of two parts. The first one is spindle speed detection and the second one is stiffness modulation ON/OFF information.

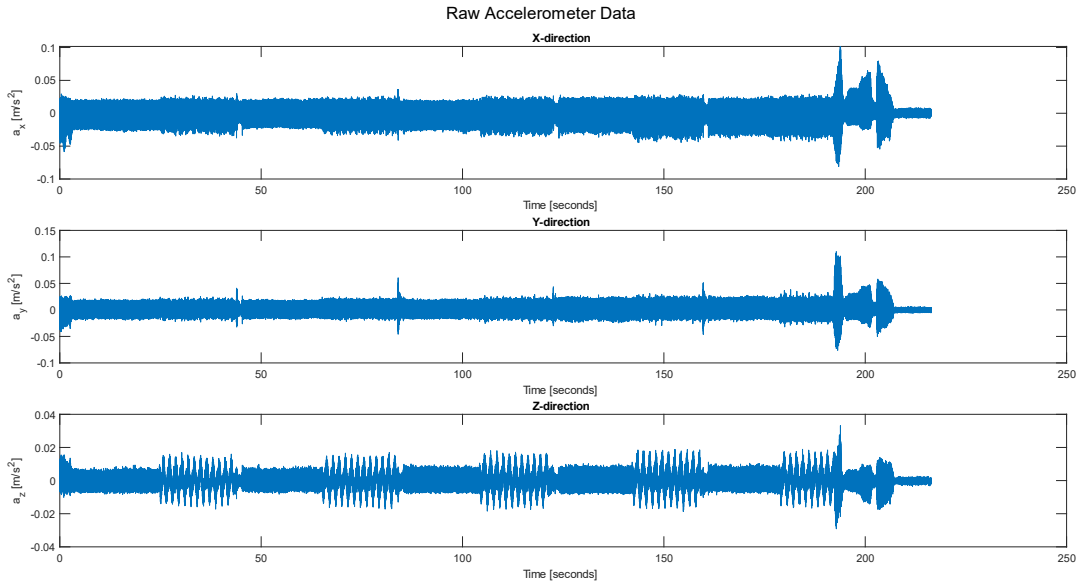

Figure 17. Raw Accelerometer Data with no Ω and SV information

4.1.1Spindle Speed Detection

The spindle speed detection algorithm works with the aim of finding dominancy of used spindle speed to other possible spindle speed and its harmonics. The omega vector consists of the spindle speeds used during the experiment as $omega = [600\ 625\ 650\ 675\ 700]$. The algorithm starts with creation of harmonics of each spindle speed as below starting from the first spindle frequency not from tooth passing frequency. Then, first 7 harmonics are chosen for comparison.

$$spf = \begin{bmatrix} 10 & 20 & 30 & 40 & 50 & 60 & 70 \\ 10.41 & 20.83 & 31.25 & 41.66 & 52.08 & 62.5 & 72.9 \\ 10.83 & 21.66 & 32.5 & 43.33 & 54.16 & 65 & 75.83 \\ 11.25 & 22.5 & 33.75 & 45 & 56.25 & 67.5 & 78.75 \\ 11.67 & 23.33 & 35 & 46.66 & 58.33 & 70 & 81.67 \end{bmatrix}$$

As mentioned earlier, spindle speed related frequencies must be dominant to other spindle speed harmonics. Therefore, power spectral density estimates are used with the help of applying in-built function of periodogram in MATLAB. Power spectral density estimates are calculated for each one second window and repeated until the end of experiment in x-direction.

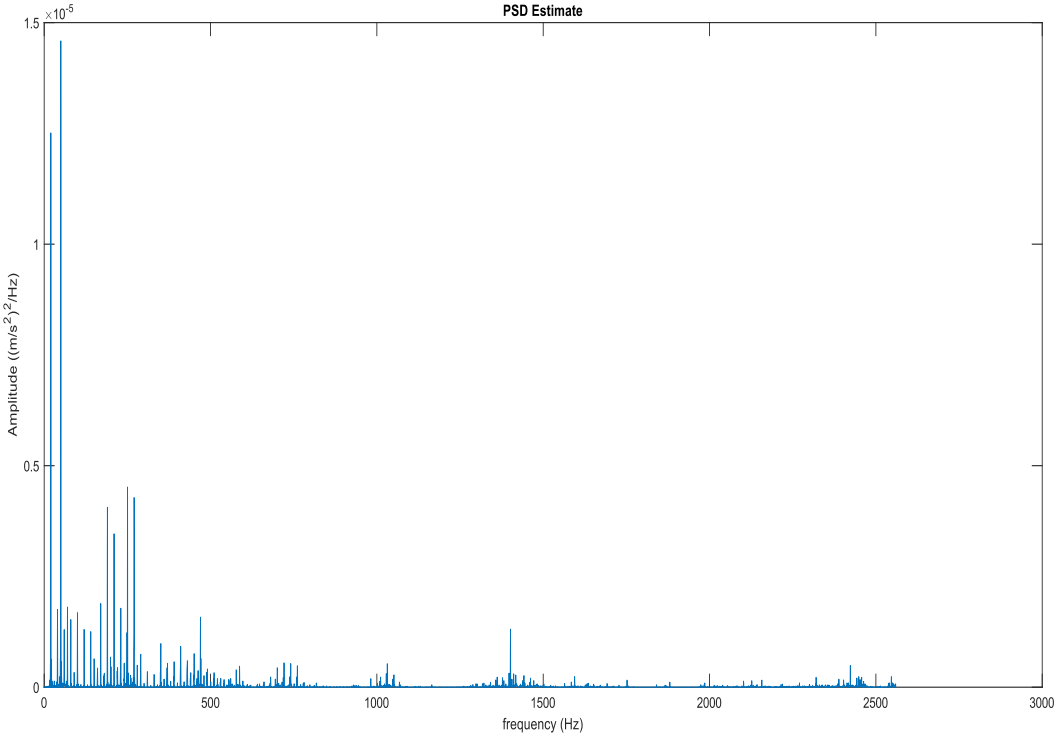

Figure 18. PSD Estimate between 0-1 second

After having the PSD estimates, the power concentrated around the spindle frequency and its harmonics can be calculated by the in-built function $bandpower$ in MATLAB which takes PSD estimate and interval to be calculated as an input. The aim is to calculate the sum of power concentrated on first 7 harmonics for each spindle speed and make a comparison between each other.

$$sum\ of\ bandpower(spf) = \begin{bmatrix} 254 \\ 10.4 \\ 4.3 \\ 2.6 \\ 16.8 \end{bmatrix} (10^{-7})$$

It can be easily understood that, in this example the highest power belongs to 600 rpm related frequencies. Therefore, the spindle speed has been decided as 600 rpm for the specified one second window. This procedure is applied in a for loop which can be seen in Appendix. At the end of this process, a plot which has different colors to represent each spindle speed.

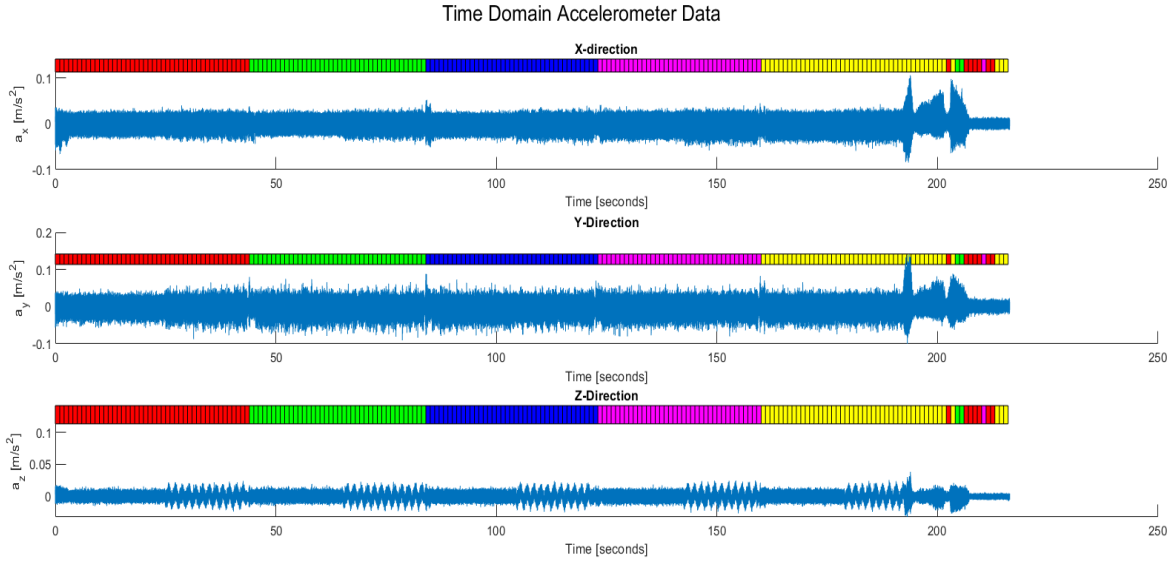

Figure 19. Time Domain Accelerometer Data with Spindle Speed Detection

4.1.2 Stiffness Variation Detection

Stiffness variation is activated in some time intervals of each second. Since stiffness modulation will cause amplitudes around harmonics of spindle speed which are not chatter related amplitudes, it must be decided that in which intervals it is active.

The algorithm uses a similar procedure like spindle speed detection. However, the modulation exists in z-direction. Therefore, there must be a visible peak on stiffness variation (SV) frequency and its harmonics in the direction of modulation. Since stiffness variation frequency $f_{sv} = 0.66\ Hz$ is known, PSD estimate must be checked around this frequency.

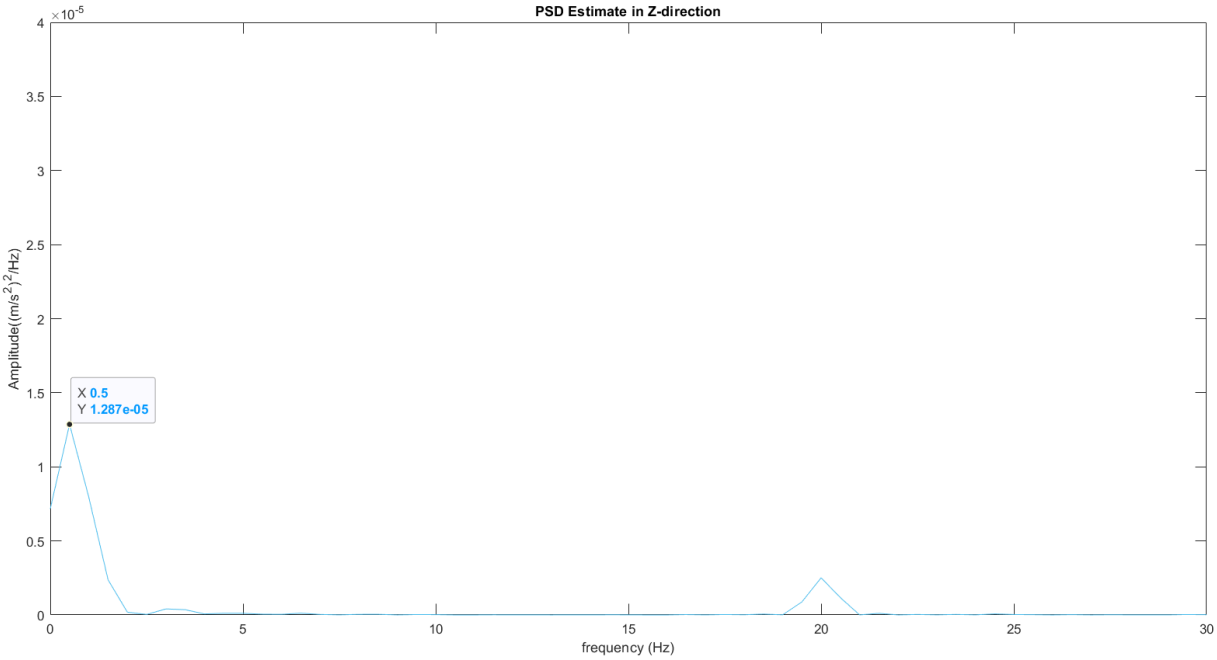

Figure 20. PSD Estimate in Z-direction

As can be in Figure 20,there is a peak around at 0.5 Hz which is close to 0.66 Hz. The difference is due to the frequency bins created by the $periodogram$ function. The number of frequency components can be increased which has the same meaning with frequency resolution by modifying the function inputs. However, since there are no expected peaks close to SV frequency, the necessity of increased resolution is eliminated by setting $bandpower$ interval between 0-2 Hz. The algorithm calculates the power of whole windowed signal and calculates the power of 0-2 Hz interval and make a ratio between them. However, setting a threshold to decide if SV is ON or OFF is a challenging task. Because the power ratio can vary due to the change of vibration. In other words, with the inclusion of regenerative contribution, the ratio cannot show the same dominance even there is a peak at SV frequency. Since the SV activation will be known during the real cutting process, it is not needed to have certain decision. Therefore, just to provide an insight of SV modulation active regions the colormap which uses the black to white scale is used in Figure 21.

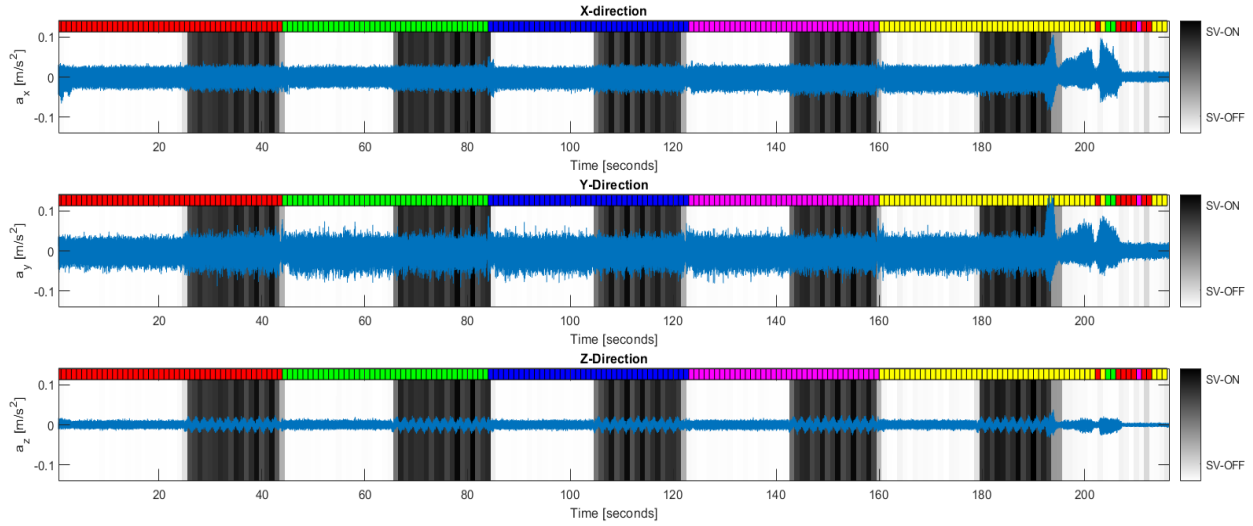

Figure 21.Black-white scale for stiffness modulation

RMS values of the signal for each second was also added to the plot to give an idea about the vibrational energy.

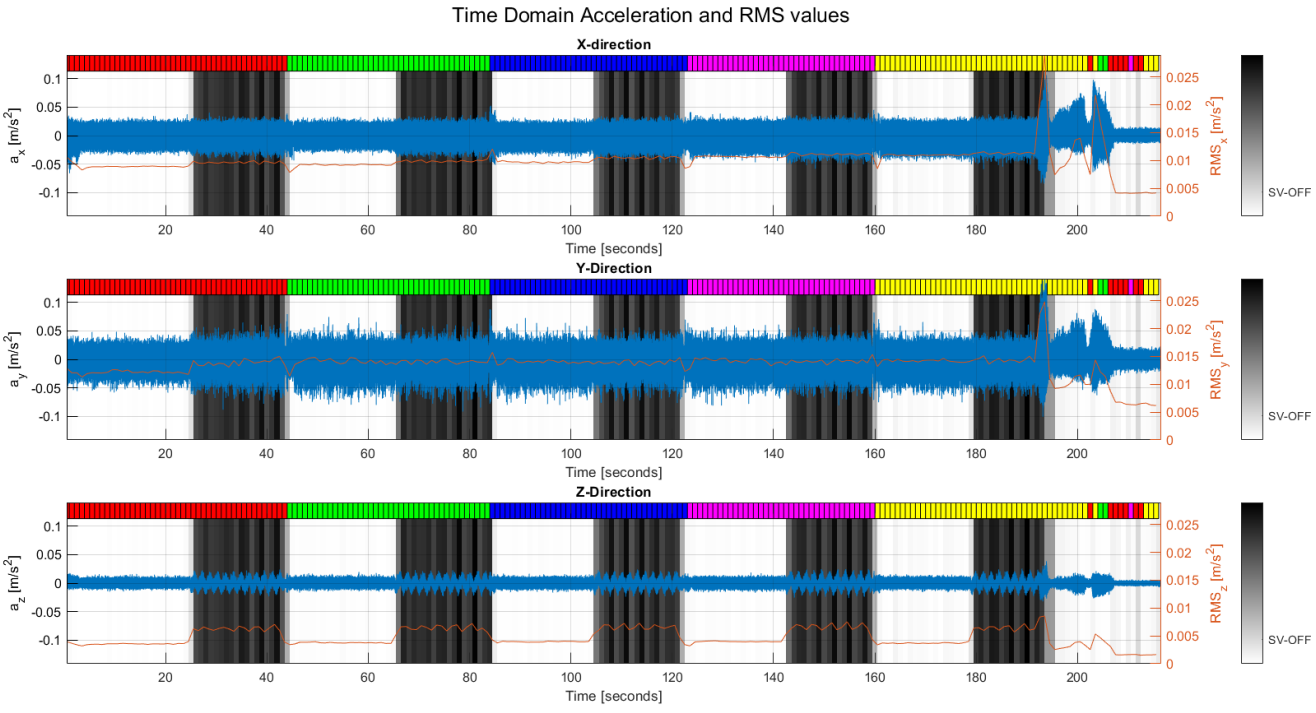

Figure 22. Spindle speed and SV detection map with RMS values

4.2 Chatter Indicator

Regenerative vibration phenomenon is different from forced vibration as discussed earlier. Tooth engagements excite the system on their own frequencies. It is expected to see peaks at these system frequencies in frequency domain. Therefore, when someone excludes these forced vibration components, the rest must belong to chatter related frequencies in other words unwanted vibration. In this project, however, there are also sidebands which are due to nature of changing dynamics. These two phenomena must be distinguished from each other sidebands and chatter respectively. Therefore, the algorithm to be applied must have two different conditions. If the SV is not active, it doesn't consider the generation of sidebands. But if SV is active, it starts to consider possible sideband generation. It can be shown as below by assuming that noise contribution is spread over the whole signal.

$$x(t) = x_p(t) + x_{ap}(t), when\ SV\ OFF$$

$$x(t) = x_p(t) + x_{sb}(t) + x_{ap}(t), when\ SV\ ON$$

where x_p is periodic components due to spindle speed harmonics, x_{ap} is aperiodic components which are unwanted vibration components and x_{sb} is the sideband contribution. A measured signal can be written as the superposition of these components.

The signal $x(t)$ is sampled at sampling frequency f_s . A window which has number of samples, N_s, is used for transition to frequency spectrum where $N_s = f_s t_w$. Window length t_w with f_s causes an optimization problem. The t_w must be chosen appropriately according to needed frequency resolution. This is well known Heisenberg-Gabor limit which emphasize increasing the number of samples will give a better resolution but causes to lose time localization that is an important concern for real-time chatter indicator. The frequency resolution generally can be computed as $f_{res} = \frac{f_s}{N_s}$. However, since computational procedure of FFT assumes the number of FFT points as power of 2, the frequency resolution is calculated also by introducing the zero padding to have a better resolution. For example, to make understanding easier, 1 second window with 5120 Hz sampling frequency.

Algorithm calculates the number of FFT points as two to the power of k that calculates the next number which is power of two greater than 5120. That is, by calculating $2^{13} = 8192$, k is chosen as 13 and N_{FFT} is decided as 8192. Therefore, by applying the formula below, frequency resolution can be calculated as 0.625 Hz.

$$f_{res} = \frac{f_s}{N_{FFT}}$$

The chatter indicator values must be evaluated for each moment set by sliding fixed window during the process and creates S_k sequence each including N_s. For having a better resolution, window length must be chosen as high as possible. Although, choosing a bigger length allows to see more robust results in the frequency spectrum, the other aim of not localizing the problematic time interval must not be overlooked. By considering the conditions mentioned above, overlapping and the length of the window must be chosen carefully.

Discussion of the FFT and uncertainty principle is one of the problems in this project. Since the basics of these terms have been given until now, the algorithm of chatter detection will be given having the basis of FFT and its restrictions in the succeeding stage. The algorithm will consist of Raw data analysis, detection of harmonics and sidebands, removal of detected components and analysis.

4.2.1Raw Data Analysis

Raw data analysis means FFT calculation of a specified window. After calculation of FFT, the variance of whole data will be calculated. Red line shows the mean value. Standard deviation of each component around mean will be calculated and squared and summed. Then, calculated sum will be divided to number of samples. The result gives the variance of the window. Since the PSD can be explained as the variance (energy) per frequency, the reason of using variance van be explained as the energy concentrated in a certain frequency component. For keeping the applied methods and calculations in sequence of equations, the result of variance calculation can be shown as

$$V_{raw} = variance(Raw\ Data)$$

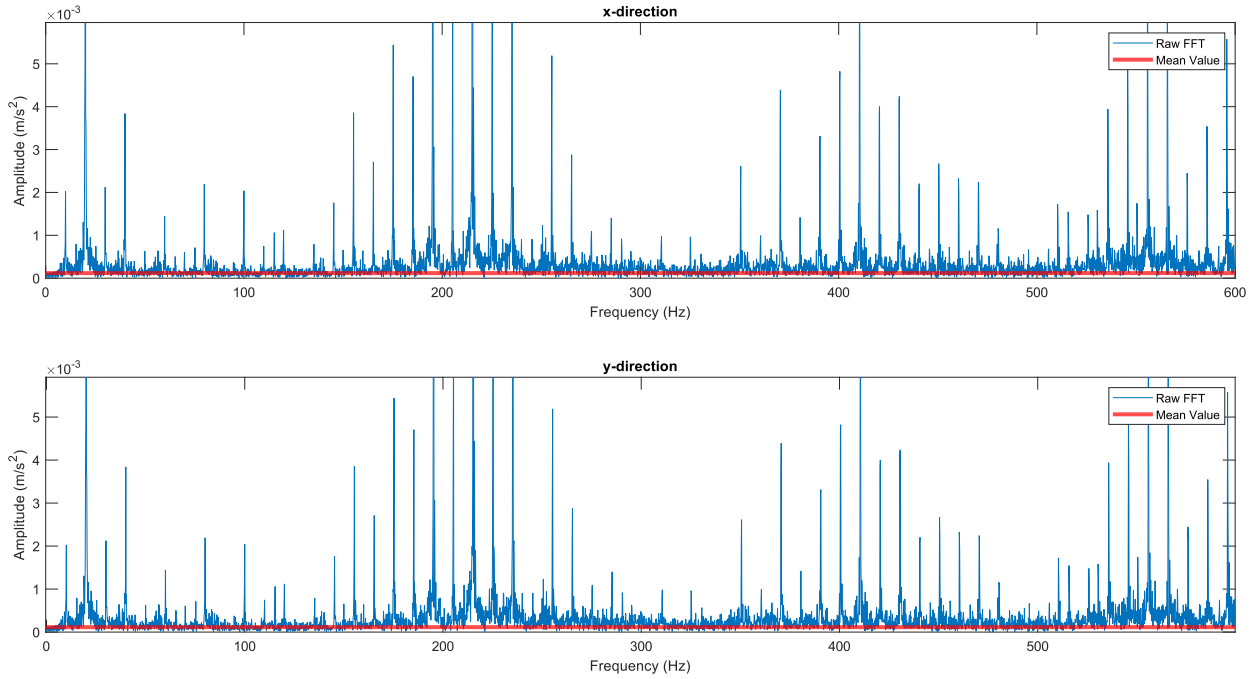

Figure 23. 5 second window FFT

4.2.2 Harmonics and Sideband Detection

Detection of the harmonics and the sidebands is the next step. If modulation is not active, sideband generation is not expected. If the SV is on sideband detection is activated. The resolution must be enough to detect the harmonics and sideband. Therefore, some different window lengths are tried to find the optimum window length. In

the set window on acceleration data and FFT of this time window when the SV is off is shown. Red asterisks show the detected spindle frequency and its harmonics. Detection of harmonic components' indexes can be shown as below where spf is calculated until dynamic range of interest, [0, 600] Hz $N_{har} = \frac{600}{spf(1)}$ where $spf(1)$ is the fundamental spindle frequency.

$$f_{har} = \frac{spf}{f_{res}} \text{ , where } [spf] \text{ is } 1 * N_{har}$$

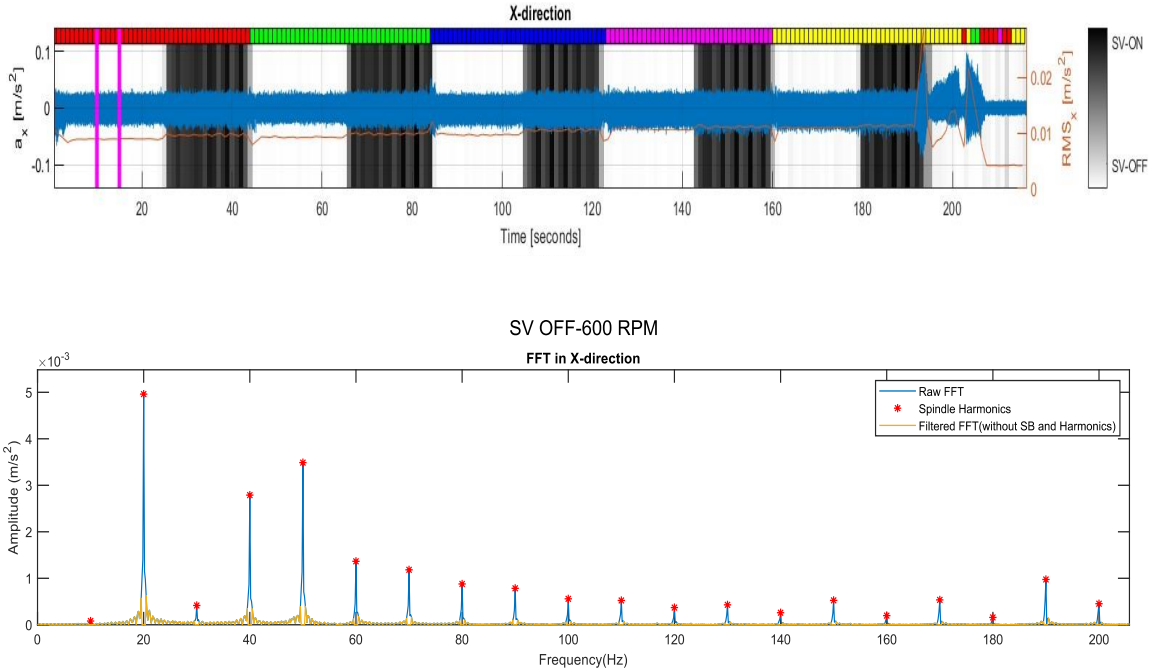

Figure 24:5 second window when SV is OFF

In Figure 25 , FFT of a time window is shown with detected spindle frequency, its harmonics and sidebands. The detection of sidebands' indexes can be shown by

$$f_{sb} = \frac{(f_{har} \pm i f_{sv})}{f_{res}},$$

where i is the number of sidebands to be considered. The magnitudes corresponding in both

and Figure 25, the magnitudes corresponding to f_{har} and f_{sb} are removed from the FFT. The residual values belong to chatter related components and are shown by yellow lines in

.

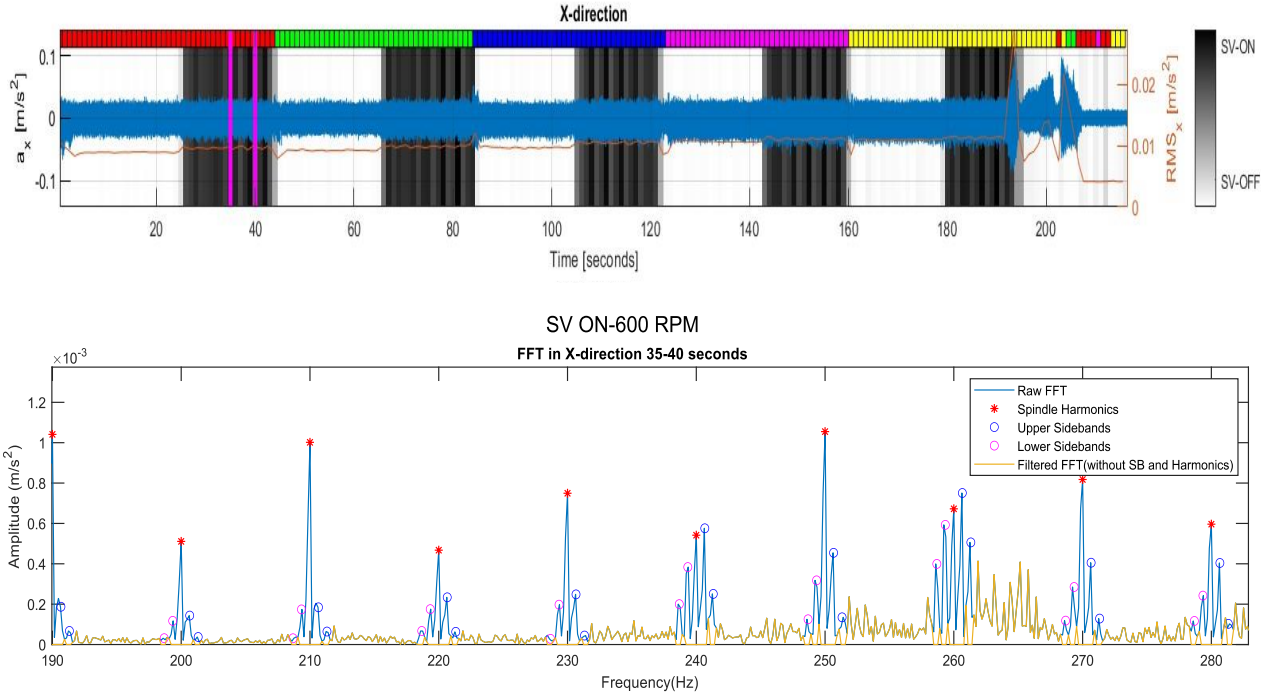

Figure 25. 5 second window when SV is ON

The FFT without sidebands and harmonics are defined as Filtered FFT in the algorithm and Filtered FFT is used for variance calculation of chatter components.

$$V_{FD} = variance(filtered\ Data)$$

As a result, the chatter indicator can be defined as the ratio between the chatter related components and the whole signal (raw data) which includes all components.

$$CI = \frac{V_{FD}}{V_{RAW}}$$

The chatter indicator calculation is performed by two accelerometer data x and y. After finding the values, a threshold was needed to set to be able to decide it is chatter or not. Threshold decision will be performed in the next chapter.

5 Results and Discussion

The chatter indicator calculation procedure for a particular window was explained in the previous chapter. The indicator must be calculated during the experiment as soon as the new data come. This is done by moving the set window and calculating the CI for new windows. The window is set as 3 seconds as lowest possible due to the frequency resolution needed. For being convenient with online chatter detection, 2.7 seconds is set as overlap value for shifting window. In other words, the last 0.3 seconds of each window belongs to new data and any increase compared to previous CI value is due to new data. Thus, a compromise between time localization and frequency resolution is aimed.

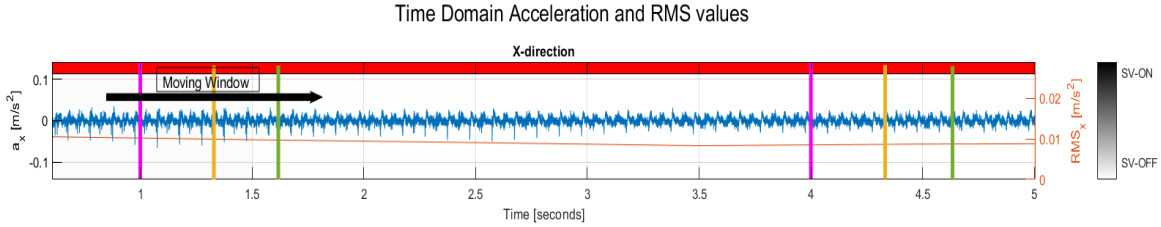

Figure 26.Moving window representation

In addition to the resolution and localization problems, setting a threshold must be done carefully. In this work, the threshold set according to recorded video and sound produced during the experiment. Some classifications are made according to these parameters as chatter, uncertain and chatter-free. On this basis, the thresholds are set and shown as below with the examined accelerometer data, indicator values and FFT plots. For setting a threshold, all the chatter indicator values are collected during the examined time region. Then RMS is applied to the indicator values and obtained one indicator value for the experiment. This is chosen as a threshold. In Figure 27 , the cutting examined between 223.5-245 second which corresponds to 650 RPM-SV ON at the depth of cut 8 mm is shown. Chatter indicator values for 3 seconds window by shifting 0.3 seconds is computed. The RMS application can be shown as $CI = RMS\ (CI_1\ CI_2 CI_3\ ....\ CI_N)$ where N is the number of chatter indicator calculation. According to this, the lower

threshold which is the border between chatter-free and uncertain region is decided as 0.55. The same procedure is applied to find the border line between uncertain-chatter region in Figure 28. The experiment conducted in Figure 28 is with 9 mm depth of cut, 625 RPM and modulation is not activated (SV OFF). Based on this experiment, the upper threshold is set as 0.85.

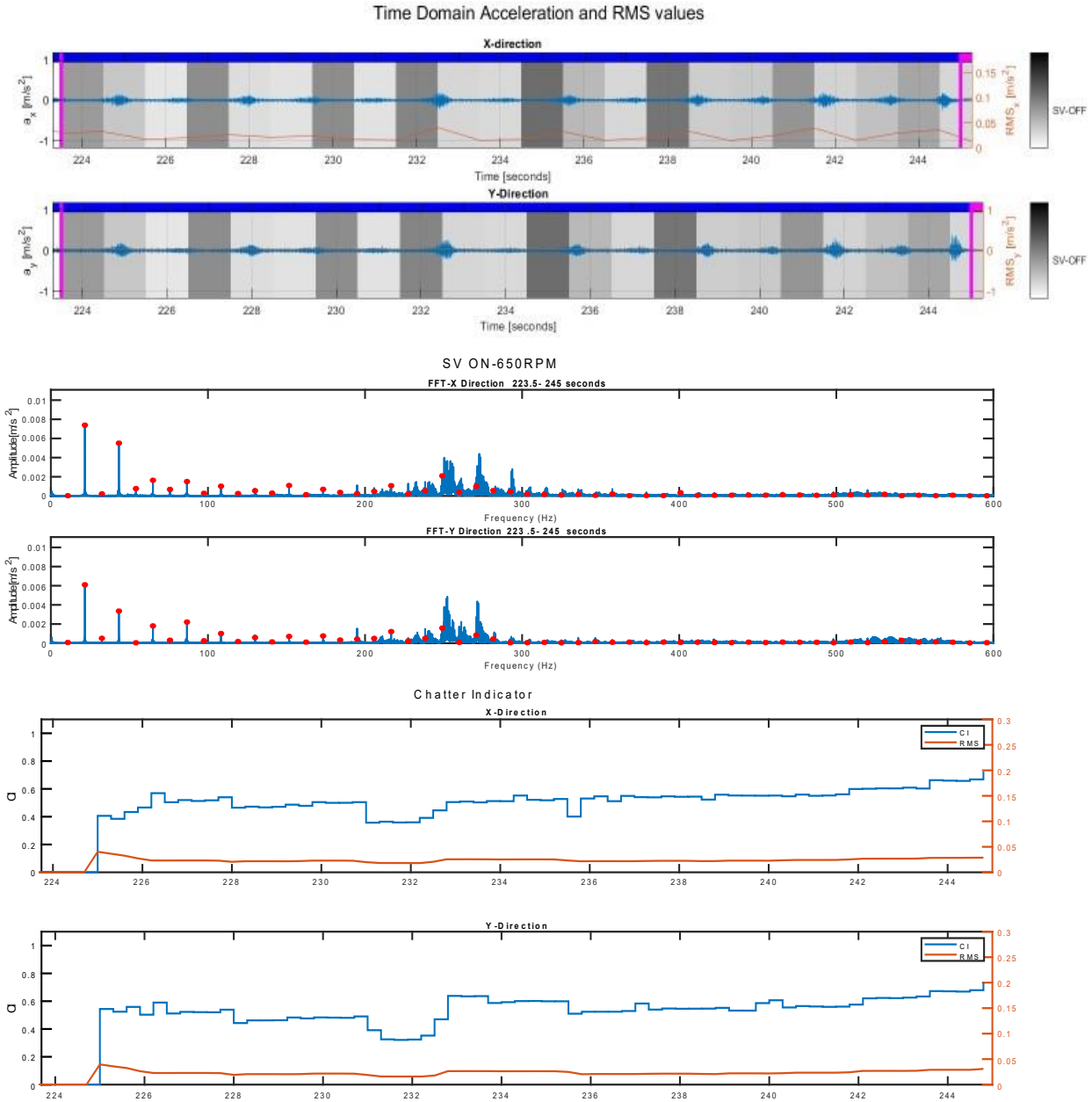

Figure 27.Vibration data, FFT and Chatter Indicator for 650 RPM-SV ON

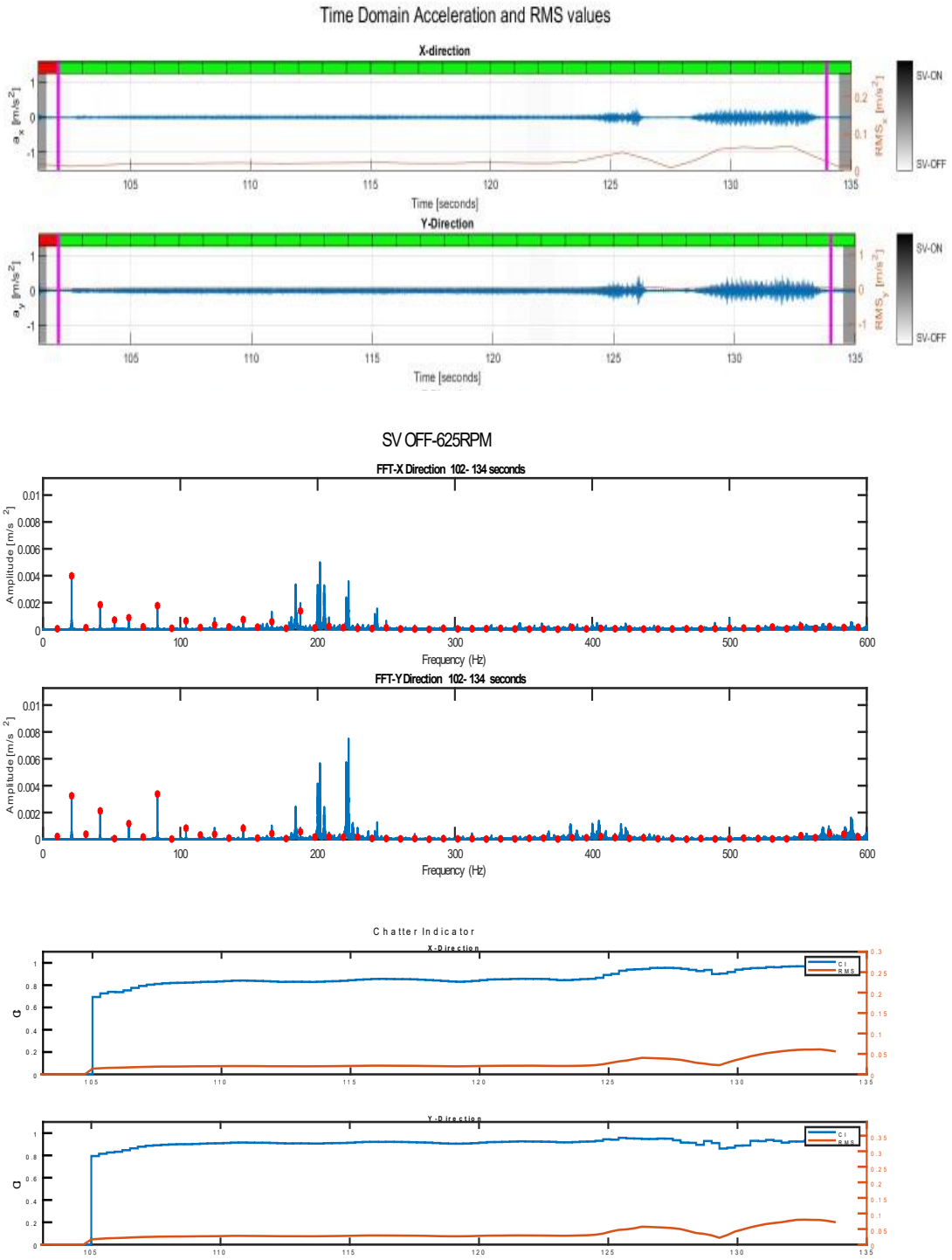

Figure 28.Vibration data, FFT and Chatter Indicator for 625 RPM-SV OFF

After setting thresholds, the results are shown as in Figure 29. The experiment was conducted with 700 RPM at the depth of cut of 9 mm. It started with no modulation and after 292.5 second stiffness modulation was activated as clearly seen in the first plot. The second plot shows the time-frequency representation of the experiment. As clearly seen, there was an energy concentration when stiffness variation was off. After starting to modulate, the discontinuity of chatter is observed. One cannot say that the situation is not chatter or chatter-free. There is uncertainty. After some time, the chatter was clearly suppressed. Therefore, all these steps must be clear in the chatter indicator plot from chatter to uncertain and uncertain to chatter-free region. Third plot which shows the chatter indicator value exactly matches with the expectations. The CI value is higher than the threshold while it gives results between 0.55-0.85 which is uncertain region. When the chatter is fully suppressed, the CI value gives results lower than the threshold. It must also be noted that if RMS was used an indicator, although CI value is low around 310 seconds, one can see the RMS increase. Therefore, it can be said that vibration is concentrated around the tooth passing frequencies even if the vibration energy increases.

In Figure 30, the stabilizing effect of stiffness variation and sensitivity and robustness of CI can be seen. High values were obtained when the SV was off. Then, with turning on the modulation, a slight decrease was observed in CI plot which matches with the time-frequency plot. Also, it must be noted that after 455 second, although it is not chatter, some energy increase was observed in time-frequency plot. This energy increase can be seen with the increase in CI value in the chatter-free region.

The real-time chatter indicator must calculate each window in a shorter time than the new window. For example, the focus is to catch the changes during the 0.3-second shift in this work. Therefore, the calculation time must be shorter than 0.3 and must give enough time for control action not to keep cutting with chatter vibration. With a simple calculation in MATLAB, the processing time was calculated as 0.02-second which shows that this algorithm is applicable in real-time.

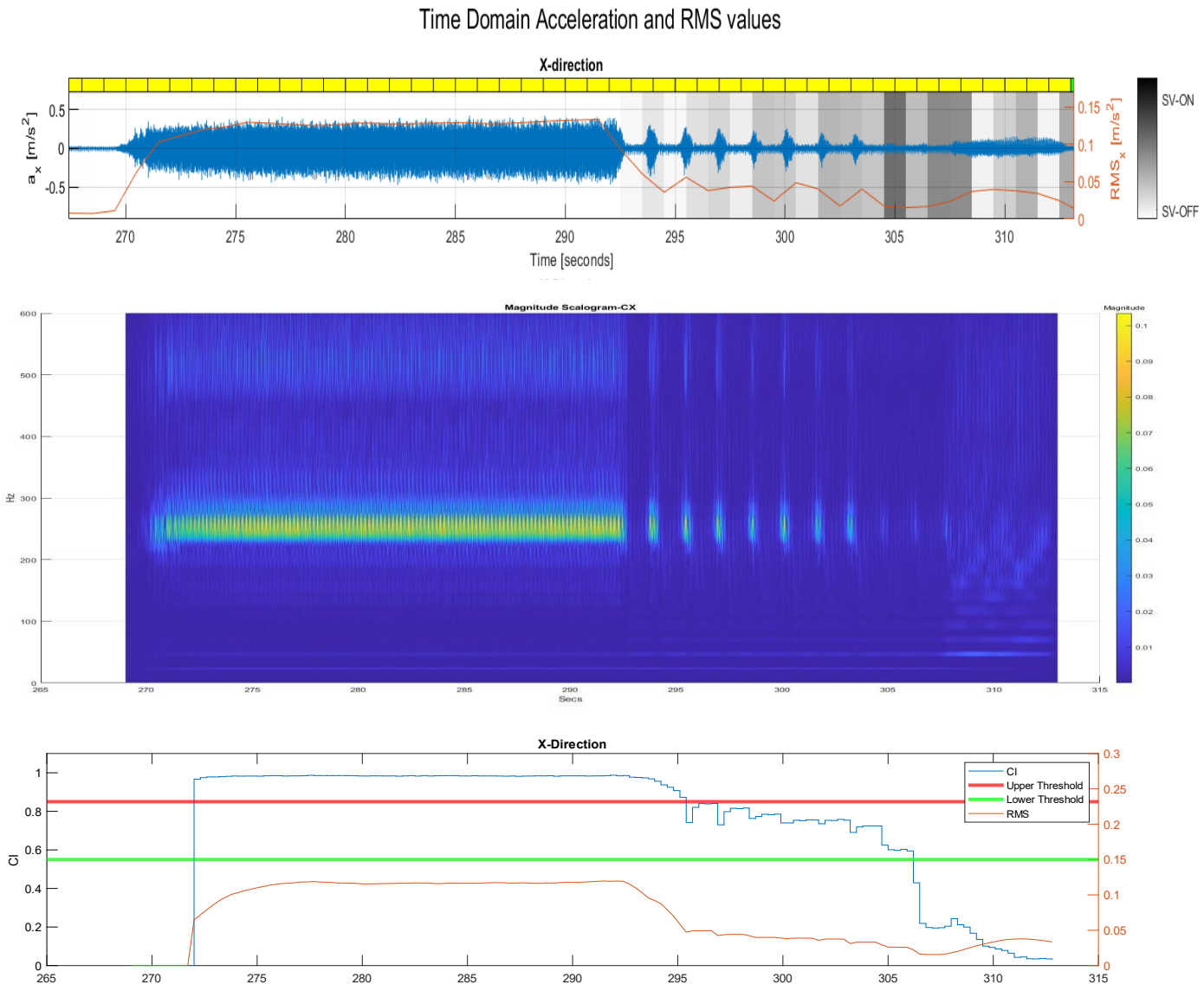

Figure 29. 700 RPM, DOC=9 mm, unstable when SV is OFF, stabile with SV ON

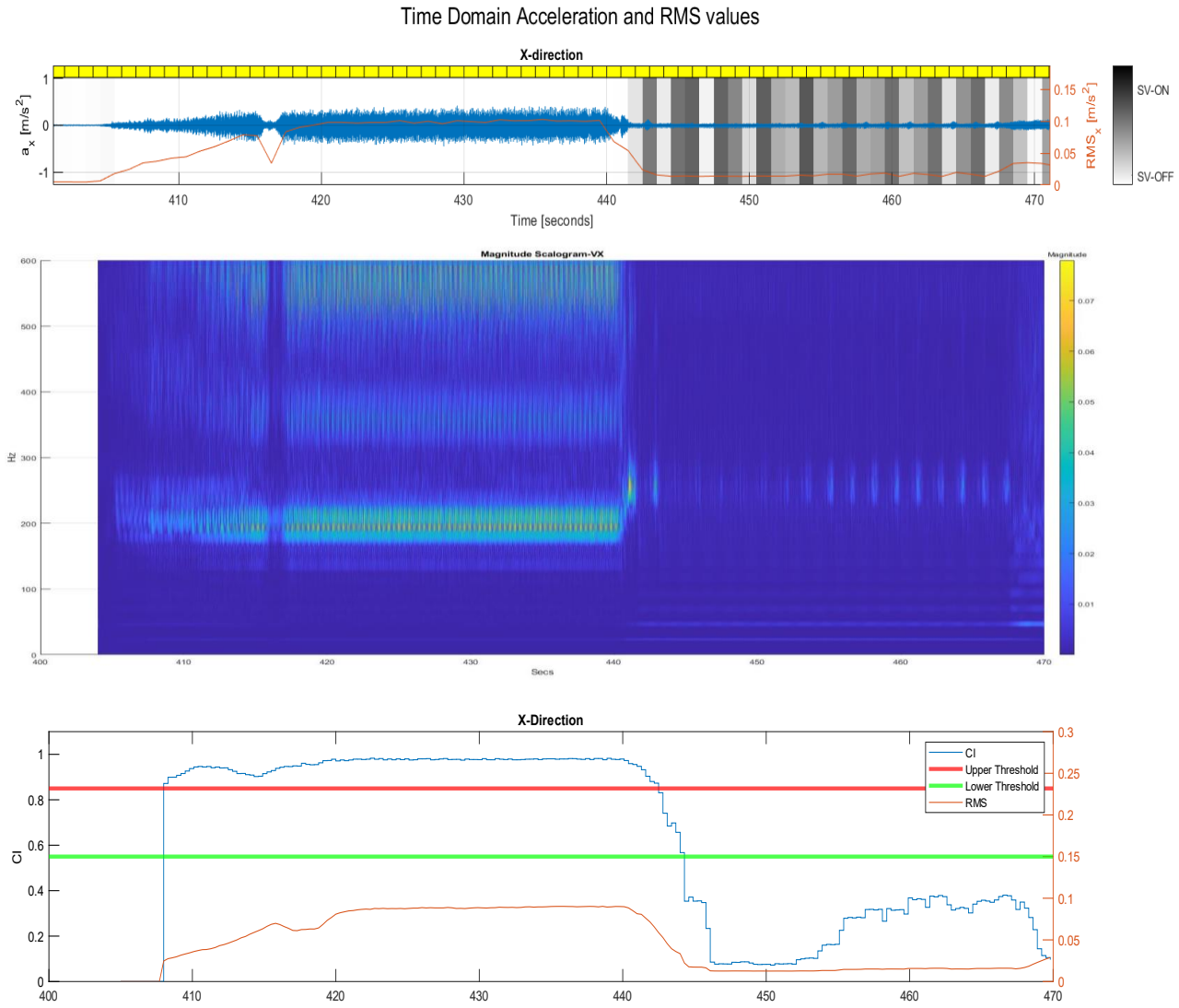

Figure 30. 700 RPM, DOC=8mm, unstable when SV is OFF, stabile with SV ON

During the assessment of the results, remarkable different results were obtained. For example, the symmetric sidebands were obtained during the earlier experiments as in Figure 25. 5 second window when SV is ON. However, on another experiment's FFT plot as in Figure 31. It has been observed that chatter frequency has also sidebands and has amplification effect on the spindle frequency and its sidebands. Also, the asymmetry is attention getting. While chatter has an amplification effect on upper part, the suppression on the opposite side has been observed. These affects must be examined in a more detailed way to have a more reliable chatter indicator value. Detecting and removing high amplitudes as in the Figure 31, might cause having a lower chatter indicator value.

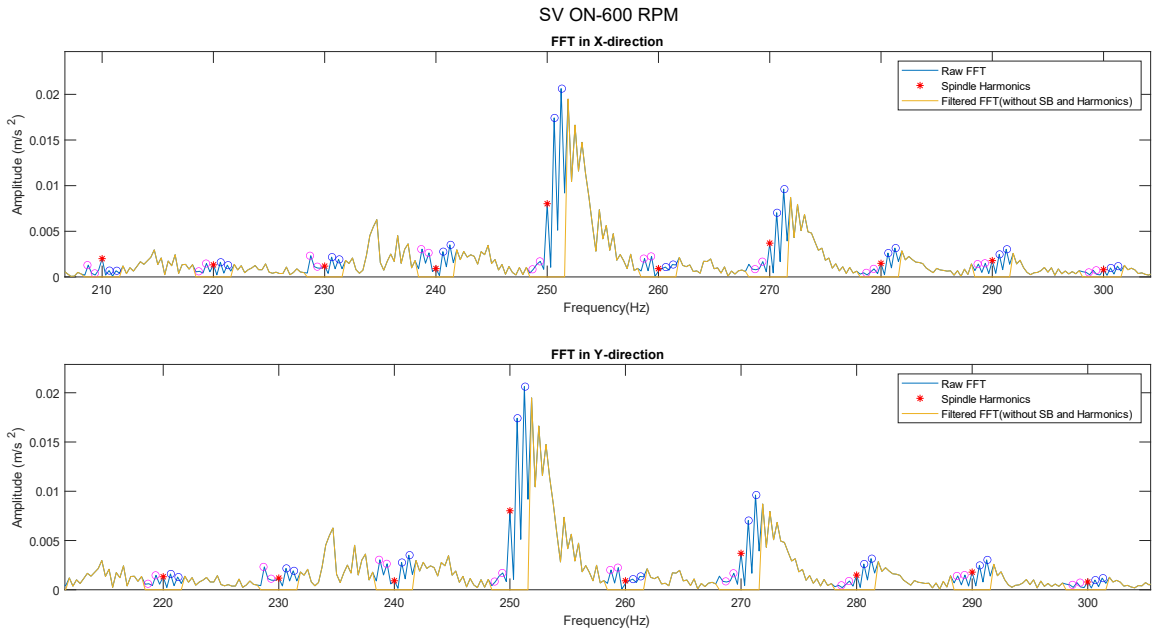

Figure 31. Asymmetric sideband formation

6 Conclusion

This study started with identifying the system's input such as spindle speed and stiffness variation status since the experimental data coming from field didn't have the recordings of this information. In MATLAB, the built-in functions periodogram and band-power were used and time domain accelerometer data was classified. After deciding the cutting speed and the stiffness variation is on or off, tooth passing frequencies were designated in the frequency domain by applying Fast Fourier Transform for feature extraction. As shown earlier, the sideband formation was observed while the modulation was active. Since the modulation frequency was known, the possible sideband frequency was introduced to the algorithm. By separating the energy components and using the ratio between synchronous and asynchronous components, the chatter algorithm was developed. The algorithm was applicable in real-time because the calculation time was low.

In future works, the sideband formation mechanism can be further examined. Because during the study, it was observed that considerable sideband magnitudes were mostly near chatter frequencies. At some cases, chatter sidebands are overlapped or suppressed. Therefore, number of sidebands to be considered should be chosen carefully. Detecting and removing magnitudes related to chatter component might lead to have wrong results. Therefore, estimating the amplitude of synchronous component's sideband amplitudes can help to have more reliable results.

Bibliography

[1] T. Akyazi *et al.*, "Skills requirements for the European machine tool sector emerging from its digitalization," *Metals (Basel).*, vol. 10, no. 12, pp. 1–23, 2020, doi: 10.3390/met10121665.

[2] Filip Geerts, "the European Machine Tool Sector and," 2019.

[3] G. Quintana and J. Ciurana, "International Journal of Machine Tools & Manufacture Chatter in machining processes : A review," *Int. J. Mach. Tools Manuf.*, vol. 51, no. 5, pp. 363–376, 2011, doi: 10.1016/j.ijmachtools.2011.01.001.

[4] L. Banda, "UCIMU: AN EXCELLENT 2021 FOR THE ITALIAN INDUSTRY OF MACHINE TOOLS, ROBOTICS AND AUTOMATION. A STRONG GROWTH ALSO IN 2022, WITH FULL RECOVERY OF THE GROUND LOST DURING THE PANDEMIC The," 2022.

[5] C. YUE, H. GAO, X. LIU, S. Y. LIANG, and L. WANG, "A review of chatter vibration research in milling," *Chinese J. Aeronaut.*, vol. 32, no. 2, pp. 215–242, 2019, doi: 10.1016/j.cja.2018.11.007.

[6] S. A. Tomas, "M A C H I N E TOOL VIBRATION RESEARCH," vol. 1, pp. 1–14, 1961.

[7] M. Thesis and C. E. Academic, "Development of an innovative solution for in-process monitoring tool and surface quality in milling operations-DOB," 2020.

[8] A. Siddiqi, "Identification of the harmonic transfer functions of a helicopter rotor," no. 1999, 2001, [Online]. Available: https://dspace.mit.edu/handle/1721.1/8900.

[9] S. Yang, "Modal identification of linear time periodic systems with applications to Continuous-Scan Laser Doppler Vibrometry," *Eng. Physics, Univ. Wisconsin-Madison*, 2013.

[10] N. Werely, "Analysis and Control of Linear Periodically Time Varying Systems." .

[11] Y. Altintaş and E. Budak, "Analytical Prediction of Stability Lobes in Milling," *CIRP Ann. - Manuf. Technol.*, vol. 44, no. 1, pp. 357–362, 1995, doi: 10.1016/S0007-8506(07)62342-7.

[12] F. Defant and P. Albertelli, "A novel harmonic solution for chatter stability of time periodic systems," *J. Sound Vib.*, no. xxxx, p. 115719, 2020, doi: 10.1016/j.jsv.2020.115719.

[13] T. Insperger and G. Stépán, "Updated semi-discretization method for periodic delay-differential equations with discrete delay," *Int. J. Numer. Methods Eng.*, vol. 61, no. 1, pp. 117–141, 2004, doi: 10.1002/nme.1061.

[14] Y. Ding, L. M. Zhu, X. J. Zhang, and H. Ding, "A full-discretization method for prediction of milling stability," *Int. J. Mach. Tools Manuf.*, vol. 50, no. 5, pp. 502–509, 2010, doi: 10.1016/j.ijmachtools.2010.01.003.

[15] M. A. Davies, J. R. Pratt, B. Dutterer, and T. J. Burns, "Stability prediction for low radial immersion milling," *J. Manuf. Sci. Eng. Trans. ASME*, vol. 124, no. 2, pp. 217–225, 2002, doi: 10.1115/1.1455030.

[16] G. Stepan *et al.*, "Nonlinear dynamics of high-speed milling - Analyses, numerics, and experiments," *J. Vib. Acoust. Trans. ASME*, vol. 127, no. 2, pp. 197–203, 2005, doi: 10.1115/1.1891818.

[17] S. D. Merdol and Y. Altintas, "Multi frequency solution of chatter stability for low immersion milling," *J. Manuf. Sci. Eng. Trans. ASME*, vol. 126, no. 3, pp. 459–466, 2004, doi: 10.1115/1.1765139.

[18] J. Gradišek *et al.*, "On stability prediction for low radial immersion milling," *Mach. Sci. Technol.*, vol. 9, no. 1, pp. 117–130, 2005, doi: 10.1081/MST-200051378.

[19] P. V Malaji and S. F. Ali, "Vibration Engineering and Technology of Machinery," *Mech. Mach. Sci.*, vol. 23, no. January 2015, pp. 411–420, 2015, doi: 10.1007/978-3-319-09918-7.

[20] J. S. Kwak and M. K. Ha, "Neural network approach for diagnosis of grinding operation by acoustic emission and power signals," *J. Mater. Process. Technol.*, vol. 147, no. 1, pp. 65–71, 2004, doi: 10.1016/j.jmatprotec.2003.11.016.

[21] H. Liu, Q. Chen, B. Li, X. Mao, K. Mao, and F. Peng, "On-line chatter detection using servo motor current signal in turning," *Sci. China Technol. Sci.*, vol. 54, no. 12, pp. 3119–3129, 2011, doi: 10.1007/s11431-011-4595-6.

[22] I. N. Tansel, M. Li, M. Demetgul, K. Bickraj, B. Kaya, and B. Ozcelik, "Detecting chatter and estimating wear from the torque of end milling signals by using Index Based Reasoner (IBR)," *Int. J. Adv. Manuf. Technol.*, vol. 58, no. 1–4, pp. 109–118, 2012, doi: 10.1007/s00170-010-2838-5.

[23] C. Liu, L. Zhu, and C. Ni, "The chatter identification in end milling based on combining EMD and WPD," *Int. J. Adv. Manuf. Technol.*, vol. 91, no. 9–12, pp. 3339–3348, 2017, doi: 10.1007/s00170-017-0024-8.

[24] K. Zhu and B. Vogel-Heuser, "Sparse representation and its applications in micro-milling condition monitoring: Noise separation and tool condition monitoring," *Int. J. Adv. Manuf. Technol.*, vol. 70, no. 1–4, pp. 185–199, 2014, doi: 10.1007/s00170-013-5258-5.

[25] T. Delio, J. Tlusty, and S. Smith, "Use of audio signals for chatter detection and control," *J. Manuf. Sci. Eng. Trans. ASME*, vol. 114, no. 2, pp. 146–157, 1992, doi: 10.1115/1.2899767.

[26] K. M. Hynynen *et al.*, "Chatter detection in turning processes using coherence of acceleration and audio signals," *J. Manuf. Sci. Eng. Trans. ASME*, vol. 136, no. 4, pp. 2–5, 2014, doi: 10.1115/1.4026948.

[27] H. Cao, Y. Yue, X. Chen, and X. Zhang, "Chatter detection in milling process based on synchrosqueezing transform of sound signals," *Int. J. Adv. Manuf. Technol.*, vol. 89, no. 9–12, pp. 2747–2755, 2017, doi: 10.1007/s00170-016-9660-7.

[28] H. Cao, Y. Lei, and Z. He, "Chatter identification in end milling process using wavelet packets and Hilbert-Huang transform," *Int. J. Mach. Tools Manuf.*, vol. 69, pp. 11–19, 2013, doi: 10.1016/j.ijmachtools.2013.02.007.

[29] H. Cao, K. Zhou, and X. Chen, "Chatter identification in end milling process based on EEMD and nonlinear dimensionless indicators," *Int. J. Mach. Tools Manuf.*, vol. 92, pp. 52–59, 2015, doi: 10.1016/j.ijmachtools.2015.03.002.

[30] Y. S. Tarng and T. C. Li, "Detection and suppression of drilling chatter," *J. Dyn. Syst. Meas. Control. Trans. ASME*, vol. 116, no. 4, pp. 729–734, 1994, doi: 10.1115/1.2899272.

[31] G. Jia, B. Wu, Y. Hu, F. Xie, and A. Liu, "A synthetic criterion for early recognition of cutting chatter," *Sci. China Technol. Sci.*, vol. 56, no. 11, pp. 2870–2876, 2013, doi: 10.1007/s11431-013-5360-9.

[32] L. Wang, J. Pan, Y. Shao, Q. Zeng, and X. Ding, "Two new kurtosis-based similarity evaluation indicators for grinding chatter diagnosis under non-stationary working conditions," *Meas. J. Int. Meas. Confed.*, vol. 176, no. February, p. 109215, 2021, doi: 10.1016/j.measurement.2021.109215.

[33] Y. Fu *et al.*, "Timely online chatter detection in end milling process," *Mech. Syst. Signal Process.*,

vol. 75, pp. 668–688, 2016, doi: 10.1016/j.ymssp.2016.01.003.

[34] Z. Zhang, H. Li, G. Meng, and S. Ren, “Milling chatter suppression in viscous fluid: A feasibility study,” *Int. J. Mach. Tools Manuf.*, vol. 120, no. February, pp. 20–26, 2017, doi: 10.1016/j.ijmachtools.2017.02.005.

[35] G. Litak, K. Kecik, and R. Rusinek, “Cutting force response in milling of Inconel: Analysis by wavelet and Hilbert-Huang transforms,” *Lat. Am. J. Solids Struct.*, vol. 10, no. 1, pp. 133–138, 2013, doi: 10.1590/s1679-78252013000100013.

[36] P. Huang, J. Li, J. Sun, and J. Zhou, “Vibration analysis in milling titanium alloy based on signal processing of cutting force,” *Int. J. Adv. Manuf. Technol.*, vol. 64, no. 5–8, pp. 613–621, 2013, doi: 10.1007/s00170-012-4039-x.

[37] Z. Yao, D. Mei, and Z. Chen, “On-line chatter detection and identification based on wavelet and support vector machine,” *J. Mater. Process. Technol.*, vol. 210, no. 5, pp. 713–719, 2010, doi: 10.1016/j.jmatprotec.2009.11.007.

[38] J. S. Kwak, “Application of wavelet transform technique to detect tool failure in turning operations,” *Int. J. Adv. Manuf. Technol.*, vol. 28, no. 11–12, pp. 1078–1083, 2006, doi: 10.1007/s00170-004-2476-x.

[39] M. Perrelli, F. Cosco, F. Gagliardi, and D. Mundo, “In-Process Chatter Detection Using Signal Analysis in Frequency and Time-Frequency Domain,” *Machines*, vol. 10, no. 1, 2022, doi: 10.3390/machines10010024.

[40] R. Teti, K. Jemielniak, G. O’Donnell, and D. Dornfeld, “Advanced monitoring of machining operations,” *CIRP Ann. - Manuf. Technol.*, vol. 59, no. 2, pp. 717–739, 2010, doi: 10.1016/j.cirp.2010.05.010.

[41] C. Liu, L. Zhu, and C. Ni, “Chatter detection in milling process based on VMD and energy entropy,” *Mech. Syst. Signal Process.*, vol. 105, pp. 169–182, 2018, doi: 10.1016/j.ymssp.2017.11.046.

[42] C. H. Chiou, M. S. Hong, and K. F. Ehmann, “The feasibility of eigenstructure assignment for machining chatter control,” *Int. J. Mach. Tools Manuf.*, vol. 43, no. 15, pp. 1603–1620, 2003, doi: 10.1016/S0890-6955(03)00185-8.

[43] G. Totis, P. Albertelli, M. Sortino, and M. Monno, “Efficient evaluation of process stability in milling with Spindle Speed Variation by using the Chebyshev Collocation Method,” *J. Sound Vib.*, vol. 333, no. 3, pp. 646–668, 2014, doi: 10.1016/j.jsv.2013.09.043.

[44] J. Munoa *et al.*, “Chatter suppression techniques in metal cutting,” *CIRP Ann. - Manuf. Technol.*, vol. 65, no. 2, pp. 785–808, 2016, doi: 10.1016/j.cirp.2016.06.004.

[45] H. Qi *et al.*, “Parameter optimization of time-varying stiffness methodfor chatter suppression based on magnetorheologicalfluid-controlled boring bar,” *Nature*, vol. 388. pp. 539–547, 2018.

[46] C. Wang, X. Zhang, Y. Liu, H. Cao, and X. Chen, “Stiffness variation method for milling chatter suppression via piezoelectric stack actuators,” *Int. J. Mach. Tools Manuf.*, vol. 124, no. 28, pp. 53–66, 2018, doi: 10.1016/j.ijmachtools.2017.10.002.